

Elasticity and Dynamics in Colloidal Dispersions.  
Particle Gel in non-Newtonian Melts  
and Stimuli-responsive Microgels

Giovanni Romeo

Advisor  
Domenico Acierno

UNIVERSITY OF NAPOLI FEDERICO II

PHD THESIS IN MATERIALS AND STRUCTURES ENGINEERING

AUTHOR  
Giovanni Romeo

ADVISOR  
Professor Domenico Acierno

UNIVERSITY OF NAPOLI FEDERICO II  
*Department of materials engineering and Production*

December 2008



# Table of Contents

<b>1</b>	<b>Introduction</b>	<b>1</b>
<b>I</b>	<b>Particle gel in non-Newtonian melts</b>	<b>7</b>
<b>2</b>	<b>Experimental</b>	<b>9</b>
2.1	Materials . . . . .	9
2.2	Preparation methods . . . . .	11
2.3	Characterization methods . . . . .	11
<b>3</b>	<b>Brownian motion: Gelation and Aging</b>	<b>15</b>
<b>4</b>	<b>Scaling of the viscoelasticity of PP-TiO<sub>2</sub> hybrids</b>	<b>23</b>
4.1	Introduction . . . . .	23
4.2	Results . . . . .	24
4.3	Conclusions . . . . .	33
<b>5</b>	<b>Refinement of the scaling: PS-SiO<sub>2</sub> hybrids</b>	<b>37</b>
5.1	Introduction . . . . .	37
5.2	Results . . . . .	38
<b>6</b>	<b>Formation and yielding of the elastic network</b>	<b>51</b>
6.1	Introduction . . . . .	51
6.2	Results . . . . .	52
<b>II</b>	<b>Thermo and pH responsive Microgel</b>	<b>61</b>
<b>7</b>	<b>Temperature dependence of elasticity and dynamics of dense microgel suspensions</b>	<b>63</b>
7.1	Introduction . . . . .	63
7.2	Experimental . . . . .	65
7.2.1	Particle synthesis and characterization methods . . . . .	65
7.3	Results . . . . .	67

7.4	Critical behavior at the LCST . . . . .	71
7.5	Conclusions . . . . .	73
<b>8</b>	<b>Microscopic dynamics</b>	<b>77</b>
8.1	Introduction . . . . .	77
8.2	Experimental . . . . .	78
8.3	Results . . . . .	81

# Chapter 1

## Introduction

Brownian motion is the evidence of thermal energy, that animates molecules and atoms, allowing them to rapidly exchange their positions, like in liquids, or to vibrate around their equilibrium position, like in solids. The amazing feature of colloids is that due to their relatively large size (it spans from few nanometers to few microns), we can directly see the effect of this molecular agitation through the motion of the colloidal particle, and this can be done with very simple methods like optical microscopy. Through colloidal Brownian motion, in fact, Einstein proved the molecular structure of matter [1].

In addition to Brownian motion, colloids experience a number of microscopic forces that generate amazing assemblies and structures of the particles [2]. These forces can be very different in nature spanning from purely entropic, to enthalpic like Van der Waals and hydrogen bonding, to electrostatic and finally to elastic [3]. The most simple case one can imagine is an hard-sphere dispersion; the inter-particle interaction is characterized by an infinite repulsion at contact. Remarkably, even in such a simple system, depending on particle volume fraction, particles organize in gas, liquid or crystal structures[4]. In fact even if at very small concentrations particles don't interact, thus behaving like gas molecules, by increasing concentration a short range order is induced; the range of the order increases until when, at volume fraction of about 0.5, a crystalline structure is reached. What is really surprising is that entropy induces order to maximize the free volume around each particle at expenses of configurational entropy. Although very simple, the hard sphere model is still subject of intense studies since it is the experimental model through which liquid theories [5], crystal mechanics [6] and crystal formation kinetic theories [7] may be proved. In addition to the equilibrium phases, also a glassy state can be obtained [4], in which the particle mobility is extremely reduced, but the structure is still that of a liquid. Colloidal glasses have been proven to be invaluable to study the particle and cage dynamics approaching the glassy state [8, 9]

Most of the technologically interesting colloidal systems are affected by more complex inter-particle forces. The DLVO (Derjaguin, Landau, Verwey, Overbeek) theory, developed during the 40's, describes the total inter-particle potential induced by the combined effects of Van der Waals attraction and electrostatic repulsion [3, 10]. The equilibrium configurations, competing to a minimum free energy, are, however, rarely reached, the particles remaining trapped in non-equilibrium states like a gel [11]. A gel is a disordered network of particles kept together by the attractive forces. The network spans the whole available volume enabling the dispersion to store elastic energy. Theories accounting for the kinetic of aggregates and gel formation are based on the pioneer work of Smoluchowsky on doublets formation [2], developed during the 20's. The structure of the aggregates has been investigated only much later, starting from the works of Weitz in the 80's [12]. He proved that the aggregates have a fractal-like structure that is, they are self similar on different length scales. The fractal dimension characterizes the openness of the flocs and depends on the modality of cluster formation [13].

Although not exhaustive, this description may already seem quite reach. However an even richer behavior can be obtained by using a macromolecular liquid as/in the suspending medium. The interactions of a polymer chain and a surface vary depending on their affinity, leading to structures whose origin are different in nature [14]. If, for example, a polymer is added to a colloidal dispersion in which the medium is a good solvent for the macromolecules and these do not adsorb on the particle surface, whose dimension is quite bigger than the chains, a depletion interaction is produced [15]. This is an effective attractive potential between the particles arising from excluded volume entropy. If instead the polymer-particle affinity is good, one chain can adsorb at the particle surface and assume different possible conformations. In general different sites of the chain will adsorb on two or more particles resulting in a polymer bridge, which is still reflected in an effective inter-particle attractive force. In both cases, the elasticity of the eventually formed particle network will mix to the viscoelastic feature of the polymer, giving rise to a complex dynamic response that depends on both particle and polymer concentrations.

Up to now the, description has been limited to rigid spherical particles. Rod or disc like colloidal particles are of extreme technological interest; the first constitute the base of liquid crystals, and the second, resulting from clay, are widely mixed to polymer melts to improve physical and mechanical properties of the hosting matrix. The thermodynamic phase behavior of these geometries is extremely rich and would be really too long to describe here.

Finally, the particle rigidity may be controlled by using organic particles obtained by cross-linking a polymer. Internally each particle resembles a polymer gel and, when suspended in a medium, the size of the particle

is controlled by the free energy of the gel which generates an effective osmotic pressure inside the particle [16]. If suspended in a good medium for the polymer, the particles swell and the inter-particle hard-sphere-like potential at contact changes from a steep to a softer repulsion. The softness depends on the relation between internal polymer concentration and osmotic pressure. Because of their internal structure, these colloidal dispersions are named microgel. Microgel properties are unique. Their size can generally be controlled by external parameters like temperature or pH [17]. This makes them technologically relevant, since the particles behave like smart materials. A microgel dispersion can be concentrated by compressing the particles and the result is a material with rheological properties reminiscent of pastes and glasses [18]. The origin of the phase behavior, particle dynamics and elasticity of the dispersion are still quite obscure and subject of intense studies.

Of course in this thesis I only touch a very small fraction of the arguments described above, mainly focusing on the microscopic origin of the viscoelastic properties of two classes of dispersions.

The first is represented by attractive particles dispersed in a polymer melt, in the case of poor polymer particle affinity. The particles are spherical and of nano-metric size. The resulting aggregates are Brownian and as a consequence can form an elastic network whose response to small deformations mixes with the intrinsic viscoelasticity of the suspending non-Newtonian liquid. Different model systems are used to give a general description of the volume fraction and frequency dependence of the linear viscoelastic moduli.

The second class is represented by concentrated microgel dispersions. The particle size is both temperature and pH dependent. I study the rheological response showing that, depending on temperature the viscoelastic response is characteristic of a glass, a liquid and a gel.

Finally in the last chapter, the microscopic dynamics of the compressed, swollen particles are analyzed. The liquid of particles approaches a glassy state as function of the degree of compression. The dynamics of the supercooled liquid are extremely rich and both structural relaxation and correlations in the cage are compared to hard-sphere counterparts.

Chapter 1

# Bibliography

- [1] Einstein, A. *Investigations on the theory of the Brownian movement*, Dover (1956)
- [2] Russel, W. B.; Saville, D. A. and Showalter, W. R. *Colloidal dispersions* Cambridge university press 1989
- [3] Israelachvili, J. *Intermolecular and surface forces* Second edition, Elsevier (1992)
- [4] Pusey P. N. and van Megen W. *Nature* 320, 340 (1986)
- [5] Hansen J. P., McDonald I. R. *Theory of simple liquids* Third Edition, Elsevier (2005)
- [6] Shall P., Cohen I., Weitz D. A. and Spaepen F. *Nature* 440, 319 (2006)
- [7] Alsayed A. M., Islam M. F., Zhang J., Collings P. J., Yodh A. G. *Science* 309, 1207 (2005)
- [8] L. Berthier, G. Biroli, J.-P. Bouchaud, L. Cipelletti, D. El Masri, D. L'Hôte, F. Ladieu, M. Pierno *Science* 310,1797 (2005)
- [9] Weeks E. R., Crocker J. R., Levitt A. C., Schofield A. and Weitz D. A. *Science* 287, 627 (2000)
- [10] Verwey E. J. W. and Overbeek J. TH. G. *Theory of the Stability of Lyophobic Colloids* Dover (1999)
- [11] V. J. Anderson, H. N. W. Lekkerkerker *Nature*, 416, 811 (2002).
- [12] D. A. Weitz, M. Oliveria, *Phys. Rev. Lett.* 52, 1433 (1984)
- [13] M. Y. Lin, H. M. Lindsay, D. A. Weitz, R. C. Ball, R. Klein, and P. Meakin, *Nature* 339, 360 (1989)
- [14] Vrij A. *Pure Appl. Chem.* 48, 471 (1976)
- [15] Asakura S. and Osawa F. *J. Chem. Phys.* 22, 1255 (1954)

Chapter 1

- [16] Flory P. G. *Principles of polymer chemistry* Cornell University press (1959)
- [17] M. J. Snowden, B. Z. Chowdhry, B. Vincent, and G. E. Morris J. Chem. Soc. Faraday Trans. 92, 5013 (1996)
- [18] M. Cloitre, R. Borrega, F. Monti, and L. Leibler Phys. Rev. Lett. 90, 068303 (2003)

## Part I

# Particle gel in non-Newtonian melts



## Chapter 2

# Experimental

### 2.1 Materials

Two polymeric matrices have been used as suspending mediums.

The first is an entangled polypropylene (PP, Moplen, HP563N by Basell) with an average molecular weight  $M_w=245$  KDa and polydispersity index  $M_w/M_N \simeq 1.9$ . The glass transition temperature  $T_g \simeq 6$  °C and melting temperature  $T_m = 169$  °C are measured by differential scanning calorimetry (DSC, TA Instruments.) at a rate of  $2.5$  °C/min.

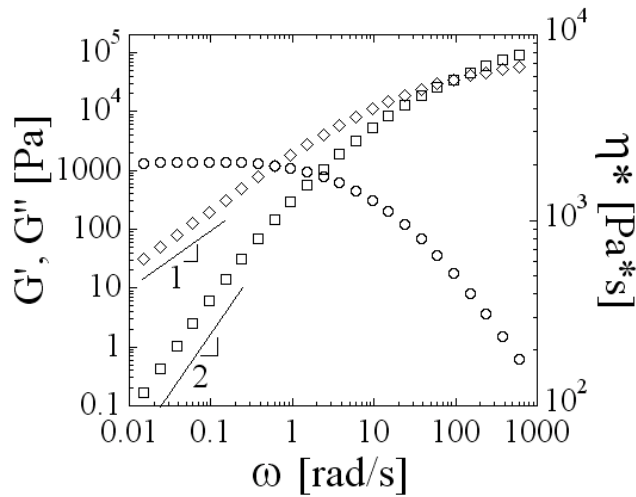


Figure 2.1: Frequency dependence of the complex viscosity  $\eta^*$  and linear viscoelastic moduli for the Polypropylene matrix.

The radius of gyration  $R_g \simeq 13$  nm in the melt is obtained from the relation  $R_g = l(1/6N)^{1/2}$  [1], where  $N$  is the number of Kuhn segments

in a chain and  $l$  is their length. The zero-frequency complex viscosity is  $\eta_o = 2 \cdot 10^3 \text{ Pa} \cdot \text{s}$  as shown in figure 2.1 where the frequency dependence of the viscoelastic moduli is also reported. The linear viscoelastic moduli approach the terminal regime at  $\omega \simeq 0.1 \text{ rad/s}$  which is well inside the frequency range investigated.

The second matrix is polystyrene (PS, polimeri Europa). We use two different molecular weights  $M_w=125$  and  $268 \text{ KDa}$ . For completeness in this section, data for an intermediate molecular weight  $M_w=192 \text{ KDa}$  are also reported. The glass transition temperature doesn't change much with molecular weight being,  $T_g \simeq 100 \text{ }^\circ\text{C}$ . All molecular weights are in the entangled regime for the PS as evident from the scaling  $\eta_o \sim M_w^{3.5}$  reported in the inset of figure 2.2. In figure 2.2 the shear rate  $\dot{\gamma}$  dependence of the viscosity is also reported together with the frequency dependence of the complex viscosity  $\eta^*$ . The linear viscoelastic moduli approach the terminal regime at  $\omega \simeq 0.1 \text{ rad/s}$  which is well inside the frequency range investigated.

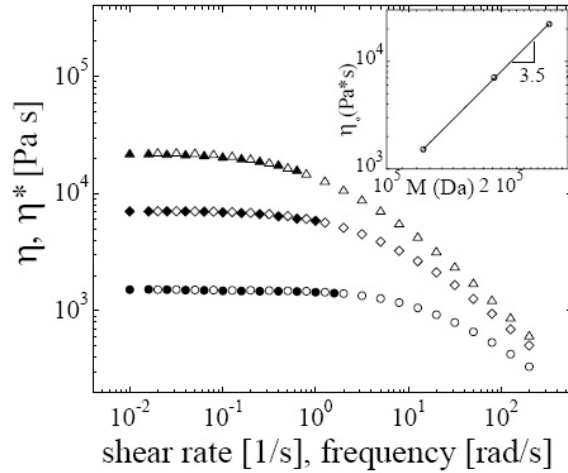


Figure 2.2: Flow curves (open symbols) for three polystyrene matrices at molecular weights  $M_w=125$  (circles),  $192$  (diamonds) and  $268$  (triangles) KDa. Solid symbols represent the complex viscosity  $\eta^*$  as function of frequency. In the inset the dependence of the zero shear viscosity is reported as function of molecular weight.

Three kinds of nanoparticles are used.

Titanium dioxide ( $\text{TiO}_2$  nanopowder by Sigma Aldrich; density:  $3.9 \text{ g/mL}$ ; surface area:  $190 \div 290 \text{ m}^2/\text{g}$ ; average primary particles diameter  $d=15 \text{ nm}$ ).

Alumina ( $\text{Al}_2\text{O}_3$  nanopowder by Sigma Aldrich; density:  $4 \text{ g/mL}$ ; surface area:  $35 \div 43 \text{ m}^2/\text{g}$ ; average primary particles diameter  $d=40 \text{ nm}$ ).

Fumed silica ( $\text{SiO}_2$  nanopowder by Degussa; density:  $2.2 \text{ g/mL}$ ; surface

area:  $135 \div 165 \text{ m}^2/g$ ; average primary particles diameter  $d=14 \text{ nm}$ ).

## 2.2 Preparation methods

Hybrids with polypropylene matrix are prepared using a co-rotating inter-meshing twin-screw extruder (Thermohaake, Rheomex PTW 24/p). Prior to mixing, the polymer and the powders are dried under vacuum for three hours at  $90 \text{ }^\circ\text{C}$ , and dosed into the extruder by using two distinct metering feeders; the filler is always added to the polymer melt. The presence of three mixing blocks along the screws ensures a good degree of powder distribution. We maintain a temperature profile ranging from  $160 \text{ }^\circ\text{C}$  to  $190 \text{ }^\circ\text{C}$  along the extruder, and collect the materials at the die exit, cooling them in water at room temperature in order to quench the internal structure of the hybrids. The diameter of the capillary die is  $2 \text{ mm}$  and the rotation frequency of the screw is set to  $\simeq 80 \text{ rpm}$ , which results in residence times of the order of two minutes.

The PS/SiO<sub>2</sub> hybrids have been prepared using a counter-rotating mini-extruder (Minilab Microcompounder, ThermoHaake). Prior to mixing, the polymer and the powders are dried under vacuum for three hours at  $90 \text{ }^\circ\text{C}$ . The residence time of the material in the extrusion chamber may be changed at will, thanks to the presence of a feed-back with a volume of  $5 \text{ cm}^3$ . The diameter of the die is  $D = 1 \text{ mm}$ . Samples are extruded at  $T=190 \text{ }^\circ\text{C}$  and the following procedure has been used: with the screws in rotation at  $50 \text{ rpm}$  half of the polymer amount is added to the chamber, then the powders are slowly loaded and finally, after about 3 minutes, the remaining polymer is added. The speed of the screws is raised to  $100 \text{ rpm}$  and after about five minutes the feed-back is opened and the material cooled down in water at room temperature.

The pure PP and PS, used as a reference in the rheological investigations, are extruded under the same conditions of the relative hybrids to allow quantitative rheological comparisons.

## 2.3 Characterization methods

The internal morphology of the hybrids is observed using transmission electron microscopy (TEM Philips, mod. EM 208). The state of filler dispersion is quantified through the analysis of many TEM images at different magnifications. All samples are microtomed using a diamond knife at room temperature in order to guarantee a thickness of  $100\text{-}150 \text{ nm}$ .

Rheological tests are carried out by means of a strain-controlled rotational rheometer (Rheometric Scientific<sup>TM</sup>, ARES L.S.) and a stress-controlled rotational rheometer (TA Instruments ARG2) using parallel plate

geometry; the diameter of the plates is either 25 mm or 50 mm. The measurements are performed in an atmosphere of dry nitrogen at  $T=190$  °C after melting the solid hybrid between the rheometer plates; the time required to do this is about three minutes, which is enough to obtain suitable disks for rheological analyses.

Oscillatory shear strain scans are performed at a fixed frequency of 0.063 *rad/s* to determine the critical strain  $\gamma_c$  that separates the linear and non-linear viscoelastic responses.

Oscillatory shear frequency scans are performed at a fixed strain in linear regime to determine the dynamical response of the samples to a small perturbation.

Application of large amplitude oscillatory shear (LAOS) for different deformation amplitudes is sometimes performed to analyze the effect of shear history on the linear viscoelastic moduli.

Low-frequency ( $\omega=0.063$  rad/s) time-sweeps are performed at a fixed strain to investigate the temporal evolution of the viscoelastic properties in linear regime.

Stress relaxation experiments consist on imposing a constant strain,  $\gamma$ , in linear regime, subsequently following the transient stress,  $\sigma(t)$ . An algorithm developed by Mead [2, 3] and that is available with the RSI Orchestrator software of the ARES rheometer is used to evaluate the relaxation-time spectra starting from the stress relaxation modulus,  $G(t) = \sigma(t)/\gamma$ . The frequency-dependent elastic ( $G'$ ) and viscous ( $G''$ ) moduli are then calculated as:

$$G'(\omega) = \sum_{i=1}^N G_i \frac{(\omega\lambda_i)^2}{1 + (\omega\lambda_i)^2} \quad (2.1)$$

$$G''(\omega) = \sum_{i=1}^N G_i \frac{\omega\lambda_i}{1 + (\omega\lambda_i)^2} \quad (2.2)$$

where  $G_i$  and  $\lambda_i$  are, respectively, the modulus and characteristic time of the  $n$  Maxwell-mode of the spectrum.

Finally, as a result of the marked sensitivity of the sample rheology on filler content, we evaluate the amount of inorganic phase in each sample by performing thermogravimetric analyses (TGA) at the end of the rheological experiments.

# Bibliography

- [1] De Gennes P.G. *Scaling concepts in polymer physics*, Cornell University Press (1979)
- [2] Mead D.W. J Rheol 38,1769-1795 (1994)
- [3] Mead D.W. J Rheol 40, 633-662 (1996)

Chapter 2

## Chapter 3

# Brownian motion: Gelation and Aging

One of the most important features characterizing the difference between nano or micro particles as fillers for a polymer melt, is the relevance of Brownian motion. To characterize how much Brownian motion is important, it's convenient to estimate the self diffusion time of a particle [1]

$$\tau_s = \frac{6\pi\eta R^3}{k_B T} \simeq 6 \cdot 10^3 \eta R^3 \text{ s} \quad (3.1)$$

at ordinary temperatures and where the solvent viscosity  $\eta$  is expressed in  $Pa \cdot sec$  and the particle radius  $R$  in  $\mu m$ . From this simple formula one easily estimates the well known result, that in simple Newtonian solvents characterized by  $\eta \simeq 10^{-3} Pa \cdot s$ , Brownian motion becomes important for particles of a few  $\mu m$ . On the contrary, since polymer melts are characterized by zero-shear viscosities of the order  $\eta_o \sim 10^3 - 10^4 Pa$ , only particles of a few tens of nanometers display a relevant Brownian displacement in the time scales of interest. The result is that, unlike for their micro-composite counterparts, polymer nano-composites are reminiscent of well known phenomenologies characterizing colloidal dispersions. When dealing with sub-micron particles dispersed in a medium, Van der Waals forces are of major importance, generally determining the stability of the system. In fact, since the refractive indexes of medium and particles are usually different, attractive forces on the nanometer scale lead to formation of aggregates and particle gel. Aggregation, gelation and phase separation in colloidal dispersions have been studied for decades both from the kinetic [1], and structural point [2, 3] of view. In this chapter I show phenomenologies of polymer nanocomposites that are easily understood in the framework of colloidal dispersions.

During extrusion hydrodynamic forces are high and can break up aggregates down to dimensions of a few particles [4]. As an example in figure 3.1 is reported the quenched mesostructure of three samples at filler volume

fraction  $\phi \simeq 0.045$  right after extrusion. The samples are made with different polymer matrices and nano-fillers; as a result the aggregates are quite different, but all of sub-micrometric dimension.

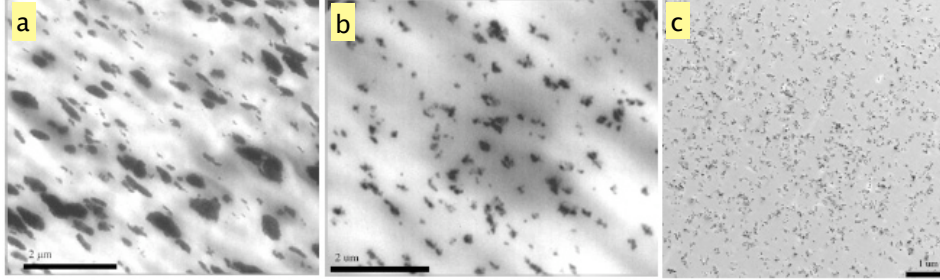


Figure 3.1: Tem micrographs of the morphologies quenched after extrusion for samples at  $\phi \simeq 0.045$ . a) PP-TiO<sub>2</sub>, b) PP-Al<sub>2</sub>O<sub>3</sub>, c) PS-SiO<sub>2</sub>.

A direct consequence of the random rearrangements of these elements, is that they assemble and build bigger structures because of Van der Waals attractions. Rheological parameters such as the linear viscoelastic moduli  $G'$  and  $G''$  are extremely sensitive to the internal microstructure and can be used to follow such internal rearrangements. We fix the frequency  $\omega = 0.063 \text{ rad/s}$  and strain  $\gamma = 0.01$  and measure how  $G'$  and  $G''$  change in time at constant temperature. Since the test is performed in linear regime, the strain applied is a small perturbation that does not affect the equilibrium morphology. The results plotted in figure 3.2 show that qualitatively the three samples share the same phenomenology: the elastic modulus increases during the first stage, reaching a plateau after a certain time  $t_a$ , while the loss modulus remains constant. Such increase of the elasticity is related to the inorganic phase, rearranging on a time scale of order  $\tau_s$ , since the neat matrices display a constant value of the moduli in time.

The morphology of the particles after aging is shown in figure 3.3. The distribution is now worse, particles and aggregates forming bigger clusters. The high values of the plateau elastic modulus suggest that at these volume fractions the particles form a whole space spanning network that can bear the stress for long times.

To further prove that the increase of the elasticity is related to network formation as a consequence of particle rearrangements, we can increase  $\tau_s$  by varying  $\eta$  or  $R$ . For high values of  $\tau_s$  we expect that the hybrid's elasticity does not significantly increase because of the reduced particle mobility. As a first test, we increase the zero shear viscosity  $\eta_o$  of the matrix by ten times, by using a high molecular weight polystyrene. In figure 3.4 we show aging curves for two hybrids obtained by mixing SiO<sub>2</sub> nanoparticles at volume fractions of 0.03 and 0.045 in such a matrix. The growth of  $G'$  is small and

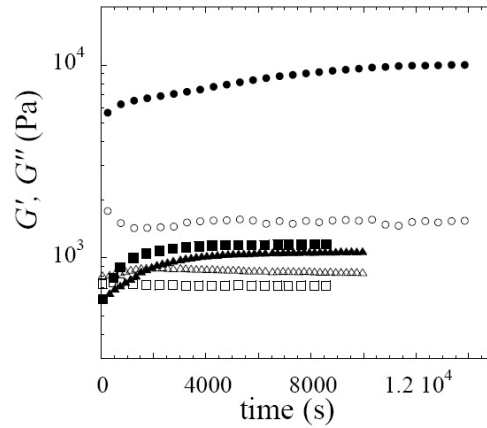


Figure 3.2: Aging curves at  $\omega = 0.063 \text{ rad/s}$  and in linear regime. PP-TiO<sub>2</sub>- $\phi=0.038$  (squares); PP-Al<sub>2</sub>O<sub>3</sub>- $\phi=0.042$ (triangles); PS-SiO<sub>2</sub>- $\phi=0.045$  (circles).  $G'$  solid symbols,  $G''$  open symbols

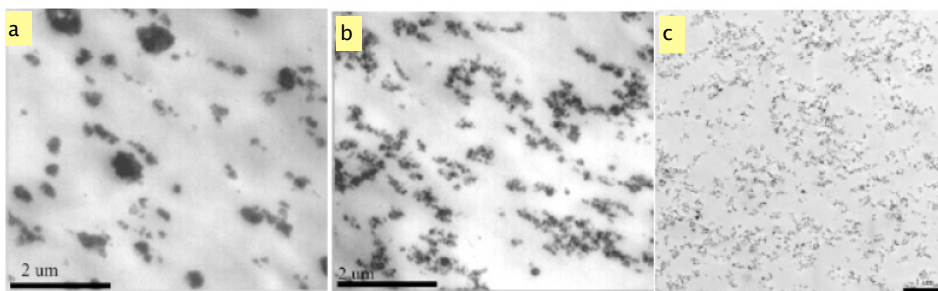


Figure 3.3: Tem micrographs of the morphologies obtained after 3 hours in quiescent state at  $T=190^\circ\text{C}$  for samples at  $\phi \simeq 0.045$ . a) PP-TiO<sub>2</sub>, b) PP-Al<sub>2</sub>O<sub>3</sub>, c) PS-SiO<sub>2</sub>.

$G''$  dominates over  $G'$  suggesting that micro-structural changes are negligible in the time scale of the test .

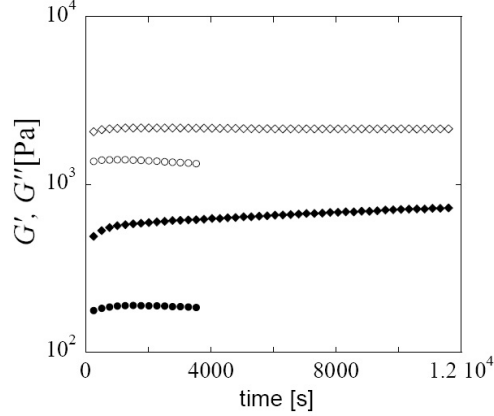


Figure 3.4: Aging curves at  $\omega = 0.063 \text{ rad/s}$  and in linear regime of a PS-SiO<sub>2</sub> sample with an high molecular weight of the matrix and at  $\phi = 0.03$  (circles) and 0.045 (diamonds).  $G'$  solid symbols,  $G''$  open symbols

To better characterize the differences emerged between the PS-SiO<sub>2</sub> hybrids, we analyze the frequency spectrum of the moduli for aged samples. The response of two hybrids at the same particle volume fraction,  $\phi = 0.045$ , but with different molecular weights of the PS matrix is shown in figure 3.5. The high frequency regime  $\omega > 1 \text{ rad/s}$  is dominated by the viscoelastic response of the matrices which show a dominating elasticity. However below the relaxation time of the polymers, the differences between the elasticities of the inorganic structures emerge. At  $\omega < 1 \text{ rad/s}$  the hybrid at high molecular weight shows a liquid-like response with the loss modulus dominating over the elastic one. On the contrary, the low molecular weight hybrid displays a clear low frequency plateau of  $G'$  which dominates over  $G''$  down to the smallest frequency investigated. Such a plateau characterizes the presence of a network that can store elastic energy for times much longer than the relaxation time of the polymer molecules.

As a second test, we use TiO<sub>2</sub> particles with radius  $R \simeq 2 \mu\text{m}$ , dispersed in the PP matrix at a volume fraction  $\phi = 0.045$ . Again, the moduli remain stable during the aging test. Also the effect over the viscoelastic response of the aged hybrids is really small when compared to the relative nanocomposite. This is shown in figure 3.6; the micro-particles induce a negligible effect over the linear viscoelastic response of the neat PP which reduces to a mere vertical shift of the moduli in the whole frequency range. This is an hydrodynamic effect that can be accounted for through the method of Gleissle [5] as will be shown in chapter 5. In the case of nanoparticles, the filler effect becomes evident at low frequencies, when the matrix elasticity

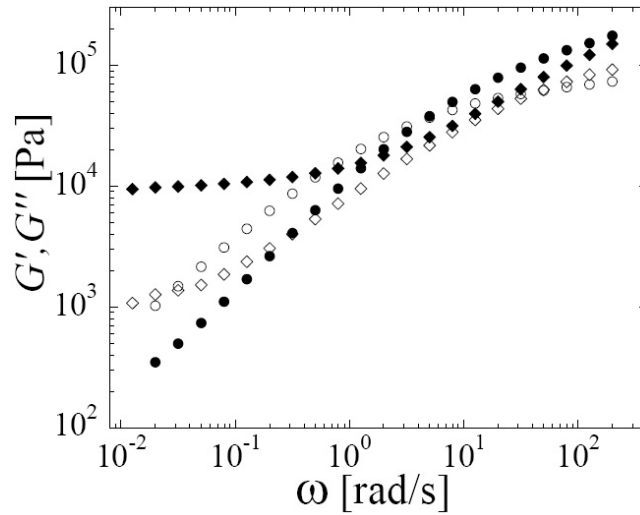


Figure 3.5: Frequency scans in linear regime of PS-SiO<sub>2</sub> samples at  $\phi=0.045$ , with two different molecular weights of the matrices: 125000 Da (diamonds); 268000 Da (circles).  $G'$  solid symbols,  $G''$  open symbols

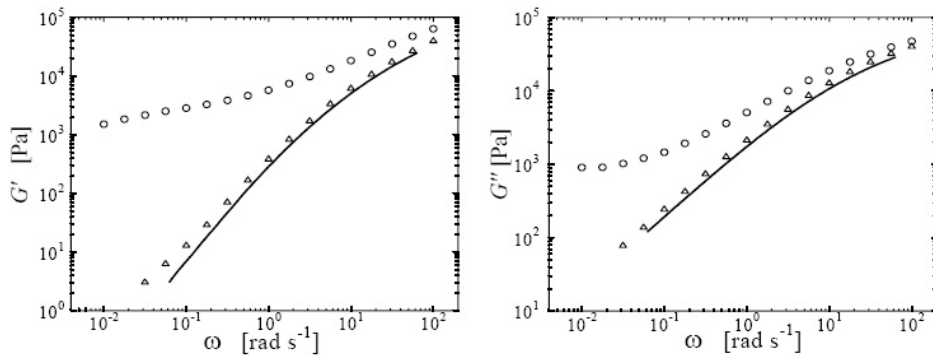


Figure 3.6: Frequency scans in linear regime of PP-TiO<sub>2</sub> samples at  $\phi \simeq 0.045$ , for micro (triangles) and nano (circles) fillers. The solid line represents the neat PP.

is negligible. Again, in this region, we find a very weak dependence of the moduli on frequency that suggests the presence of a network.

To summarize, the viscoelastic response of a filled polymer is highly affected by the particle mobility. When the diffusion time of particles and aggregates formed after the extrusion is too high, the clusters remain isolated and produce a small perturbation of the polymer viscoelastic response. When the particle or aggregates mobility is enhanced, random motion and attractive Van der Waals forces lead to assembly of the primary aggregates and eventually to formation of a whole space spanning network. Since the network is a solid, a plateau of the elastic modulus emerges at low frequencies, characterizing the elastic energy storage for long times.

# Bibliography

- [1] Russel, W. B.; Saville, D. A. and Showalter, W. R. *Colloidal dispersions*  
Cambridge university press 1989
- [2] D. A. Weitz, M. Oliveria, Phys. Rev. Lett. 52, 1433 (1984)
- [3] M. Y. Lin, H. M. Lindsay, D. A. Weitz, R. C. Ball, R. Klein, and P.  
Meakin, Nature 339, 360 (1989)
- [4] Baird, D. G.; Collias, D.I. Polymer processing principles and design  
Butterworth-Heinemann 1995.
- [5] Gleissle W. and Hochstein B., J Rheol 47, 897 (2003)

Chapter 3

## Chapter 4

# Scaling of the viscoelasticity of PP-TiO<sub>2</sub> hybrids

### 4.1 Introduction

Polymers filled with inorganic particles receive industrial and scientific attention over more than 50 years [1]. When the characteristic filler particle size is on the nanometers scale, polymer-nanocomposite systems (PNS) are formed. A general feature characterizing PNS is the significant increase of the viscoelastic properties of the hosting polymers upon addition of even extremely low loadings of nanoparticles [2, 3]. Such enhancement generally arises from the presence of a three dimensional network that may result from either direct interaction between particles [3, 4] or from inter-particle polymer-bridging mechanisms [5, 6]. For this reason, continuum rheological models [7] that successfully capture the main features of polymers filled with micron-sized particles break down when the composites are nano-structured. Furthermore, when compared to colloidal suspensions with low viscosity matrices, a higher complexity stems from the viscoelastic nature of the suspending medium and from the wide variety of microstructures and possible dynamics that arise from these multiple particle-particle [2] and polymer-particle interactions [5]. Because of this high complexity, a general description of how the frequency dependent storage and loss moduli,  $G'(\omega)$  and  $G''(\omega)$ , vary with the filler volume fraction,  $\phi$ , is still poorly understood and controversial. A possible starting point is provided by colloidal suspensions in Newtonian fluids, where new complexities can be added step by step. In these simpler systems, the arrest of particle dynamics leads to a kinetic phase transition from a liquid-like to a solid-like state; this can happen in several disparate ways and always leads to a disordered solid. For instance, at high  $\phi$  crowding of hard sphere particles results in a colloidal glass, whose solid-like features originate from the trapping of individual particles within the cages formed by the nearest neighbours [8]. At much lower volume

fractions, inter-particle attractions can cause the formation of clusters of particles and eventually a colloidal gel interspersed within the suspending medium [9]. From the knowledge of the phase behavior [10], the dynamics [11] and rheology [12] of these systems has been understood through a model that combines the elasticity of the particle network and the viscosity of the suspending liquid.

In this chapter we generalize this approach to the case of a viscoelastic medium in which the enthalpic interaction between the polymer chains and the nano-sized suspended particles may be neglected. We explain the drastic increase of  $G'(\omega, \phi)$  and  $G''(\omega, \phi)$  at low  $\omega$ , generally characterizing PNS, without eluding to polymer bridging mechanisms. We show that the complex variation of the moduli with  $\phi$  can be dramatically simplified by separating the particle network and the matrix contribution to the elasticity, as a result of the different temporal relaxation scales. We prove that the onset of the particle network exhibits critical behavior as a function of a rescaled  $\phi$ , reminiscent of elasticity percolation [13, 14]. The critical behavior of the elasticity at the percolation threshold  $\phi_c$  is due to crowding of particle clusters. Above the percolation transition, the crowding is reflected in a long-time structural relaxation that depends on particle volume fraction  $\phi$ . During these structural rearrangements we find a  $\phi$  independent glass-like relaxation mechanism where the elastic modulus,  $G'$ , scales with frequency, as  $G' \sim \omega^{0.3}$ .

## 4.2 Results

The internal microstructure of the quenched PNS is visualized using TEM. The nanohybrids at  $\phi=2.4\%$  and  $\phi=3.8\%$ , consist of sub-micron sized clusters interspersed in the polymer matrix, as shown in figure 4.1 a-b. We emphasize that the spatial distribution of the clusters is most likely not representative of their state in the melt, since TEM observations are performed over solid samples. Each cluster consists of several primary particles, which are highly packed inside the aggregate.

We measure the area,  $A_i$ , occupied by each cluster and take as representative cluster size,  $D_i$ , the diameter of a circle with the measured area of the cluster. In this way, we can construct the normalized cluster size distribution (CSD) and determine the number-average cluster-size,  $\bar{D} = \frac{\sum_i N_i D_i}{\sum_i N_i}$ , with  $N_i$  the number of clusters of size  $D_i$ . The CSD for samples with  $\phi=2.4\%$  and  $\phi=3.8\%$  is determined measuring the area of  $\sim 300$  clusters in various TEM images of the same sample; the results are shown in figure 4.1 c-d. The distributions are broad and are not very much affected by the filler content; the average size of the clusters only slightly grows from  $\bar{D} \sim 135$  nm at  $\phi=2.4\%$  to  $\bar{D} \sim 150$  nm at  $\phi=3.8\%$ . As a result, the increased filler volume fraction mainly results in an increased number of clusters, which causes a

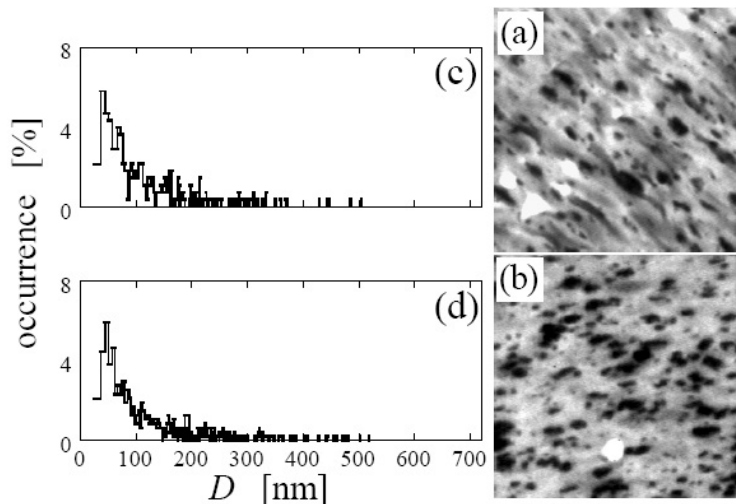


Figure 4.1: TEM micrographs of the as extruded samples at  $\phi=2.4\%$  (a) and  $3.8\%$  (b). The corresponding cluster sizes distributions are shown in (c) and (d) respectively.

reduction in the cluster-cluster mean separation distance.

In the melt, after extrusion, the clusters evolve in time. We monitor such internal rearrangements by imposing a low-frequency ( $\omega=0.063$  rad/s) oscillatory shear in the linear regime and measuring the elastic and loss moduli as a function of time. The results at  $190$  °C are plotted in figure 4.2 for three representative particle volume fractions. At  $\phi=2.4\%$ , there is no evolution of the moduli suggesting that microstructural changes, if any, do not affect either the elasticity or the viscosity of the bulk material. At this volume fraction, the sample is predominantly viscous, with  $G'' > G'$ . At  $\phi=3.4\%$ , the storage modulus slowly and slightly increases with time, almost reaching  $G''$ , which remains stable during the test. At even larger volume fractions, however,  $G'$  dramatically increases in time, eventually overcoming  $G''$  and reaching a final plateau value at some time  $t_a$ . As an example, we show in figure 4.2 the moduli for  $\phi=3.8\%$ ; in this case  $t_a \approx 4 \cdot 10^3$ s.

The increase of  $G'$  for  $\phi \geq 3.4\%$  must be related to the presence of the inorganic phase, since it is never observed for the neat polymer alone. We thus hypothesize that the clusters grow, rearrange and crowd giving rise to a space-spanning network. Formation of a network is necessary in order to cause the observed increase of sample elasticity; if clusters remain isolated, rearrangements alone cannot significantly change the elasticity of the whole system. This hypothesis is supported by evaluating the Smoluchowski time [15] for two clusters to come at contact, which we roughly estimate for the

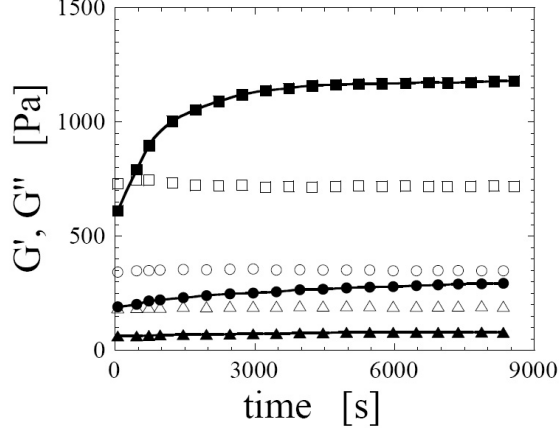


Figure 4.2: Temporal evolutions of  $G'$  (full symbols) and  $G''$  (empty symbols) at  $\omega=0.063$  rad/s for the samples at  $\phi = 2.4\%$  (reverse triangles),  $3.4\%$  (circles) and  $3.8\%$  (squares).

sample at  $\phi=3.8\%$  using the relationship

$$t_a = \frac{\pi\eta_s\bar{D}^3}{8\bar{\phi}k_B T} \quad (4.1)$$

where  $\eta_s$  is the viscosity of the suspending medium,  $k_B$  is the Boltzmann constant and  $\bar{\phi}$  is the volume fraction of the clusters. We set  $\eta_s = 2 \cdot 10^3$  Pa·s, which is the zero-shear viscosity of the neat PP, and  $\bar{D} = 150$  nm, as determined by TEM. To estimate  $\bar{\phi}$ , we assume that the primary particles are highly packed inside the clusters, as suggested by the TEM images; we thus consider that each cluster consists of primary particles packed at a volume fraction of  $\sim 60\%$ , which is close to random close packing. Then we get  $\bar{\phi} = \phi/0.6 = 6.3\%$ . Using these values, we obtain  $t_a \approx 4 \cdot 10^3$  s, which is in good agreement with the result shown in figure 4.2.

Despite the low filler content and the low polymer-particle affinity, the filler greatly affects the rheological properties of the hybrids. This is further reflected in the frequency dependence of both  $G'$  and  $G''$ , which we show in figure 4.3 for  $\phi=3.8\%$  and also for the neat polymer. The measurements are performed after 2 hours of equilibration time, which is enough to reach the stationary state values of the moduli (see figure 4.2).

The neat polymer is predominantly viscous throughout the whole frequency range and exhibits the terminal behavior of a viscoelastic fluid,  $G' \sim \omega^2$  and  $G'' \sim \omega^1$ , for  $\omega < 1$  rad/s, with a crossover at  $\omega \simeq 10^2$  rad/s reflecting the dominant relaxation mode of the polymer. In marked contrast with this behavior, the presence of multiple crossovers characterizes the viscoelasticity of the hybrid. We note, however, that the high-frequency

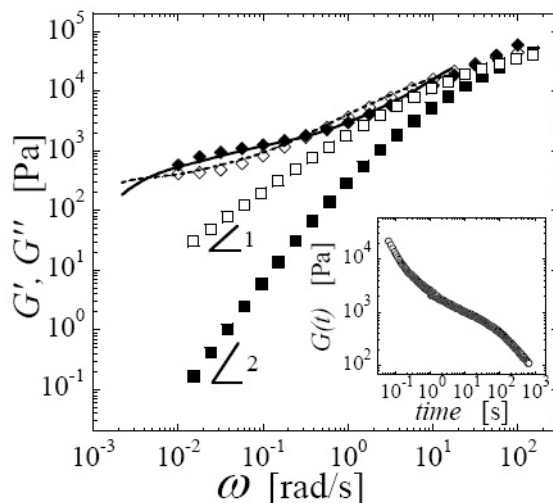


Figure 4.3: Frequency dependencies of  $G'$  (full symbols) and  $G''$  (empty symbols) obtained from frequency scan for the neat polymer (squares) and the PNS at  $\phi=3.8\%$  (diamonds). The lines represent  $G'$  (solid line) and  $G''$  (dashed line) for the PNS obtained by Fourier transforming its stress relaxation modulus,  $G(t)$ , which is shown in the inset.

( $\omega > 10^1$  rad/s) relaxation behavior of the PNS approaches that of the neat polymer, suggesting that the relaxation modes of the polymer chains and sub-chains are only slightly affected by the presence of the filler at these high frequencies [3]. For intermediate frequencies ( $10^{-2} < \omega < 10^1$  rad/s), the viscoelastic response of the hybrid exhibits a much weaker frequency-dependence as compared to the pure polymer. Such a pseudo-solid-like behavior characterizes the viscoelasticity of polymer/layered-silicates nanocomposites and it is generally explained assuming the existence of a filler space-spanning network [2, 3, 16]. The absence of a clear low-frequency plateau for  $G'$  suggests that instead of a permanent filler network, our hybrids consist of a transient three-dimensional structure, which slowly and continuously relaxes with a broad spectrum of relaxation times [17, 18]. To further explore this unexpected feature, we vary the nanoparticle volume fraction within the range  $0 \leq \phi \leq 0.64\%$  and measure the frequency dependence of the viscoelastic moduli. The results are shown in figure 4.4.

Irrespective of the frequency, both moduli increase monotonically with increasing filler loading, although, as noted earlier, the faster relaxation modes of the hybrids are essentially those of the polymer melt. The viscoelastic response of the hybrids is mainly altered, with respect to that of the PP, at low frequencies, where  $G'$  and  $G''$  exhibit weak frequency-dependences. Interestingly, in agreement with the time-dependent behavior

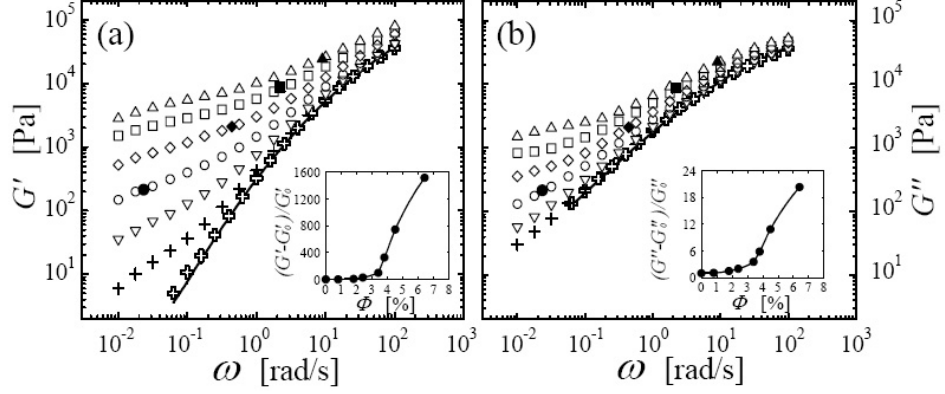


Figure 4.4: Frequency dependencies of  $G'$  (a) and  $G''$  (b) for samples at different  $\phi$ : neat polymer (solid lines), 0.8% (crosses), 1.8% (plus), 2.4% (reverse triangles), 3.4% (circles), 3.8% (diamonds), 4.5% (squares), and 6.4% (triangles). Full symbols indicate the low-frequency crossover points occurring at  $\phi \geq 3.4\%$ . The insets show the relative increase of the hybrid moduli at  $\omega=0.063$  rad/s with respect to those of the neat polymer ( $G'_o$  and  $G''_o$ ) as a function of  $\phi$ .

of the moduli (figure 4.2), the effect of the filler only becomes significant in these experiments for  $\phi \geq 3.4\%$ . This is clearly appreciated in the insets of figure 4.4 a-b, where we plot the relative increase of both moduli with respect to those of the neat polymer as a function of  $\phi$ , for  $\omega=0.063$  rad/s. Since the increase of  $G'$  is much more sensitive to the filler content than that of  $G''$ , the moduli of the hybrids at  $\phi \geq 3.4\%$  further cross at lower frequencies as shown by the solid symbols in figure 4.4. Both the cross-over frequency,  $\omega_{cl}$ , and the cross-over modulus,  $G_{cl}$  at this cross-over increase with filler content. The resultant viscoelastic behavior is reminiscent of the behavior of attractive colloidal gels in a Newtonian matrix [12]. In this simpler system, the dependence of the elastic modulus with filler content scales along the fluid viscosity as a result of the increase of the network elasticity with  $\phi$ . We follow a similar approach for our samples and consider that the main contribution to the elasticity of the hybrids at low frequencies arises from the number of elements contributing to the filler structure. Interspersed throughout this structure is the polymer, which has an intrinsic, filler-independent viscoelastic response that mixes with the network dynamics giving rise to the complex frequency and volume fraction dependences shown in figure 4.4. Despite this complexity, however, because of the differences in temporal relaxation scales of the filler network and the polymer melt, the viscoelasticity of the hybrids can be approximately decomposed into the independent responses of the elastic particle network, primarily de-

pendent on filler content and governing the long time scale response, and that of the suspending medium, dominating the high-frequency behavior.

Within this simple picture, the network elasticity will eventually equal the viscous contribution of the polymer matrix, and the previously discussed additional crossover sets the elasticity of the network. Hence, shifting the curves for  $\phi \geq 3.4\%$  with respect to  $G_{cl}$  and  $\omega_{cl}$  should lead to their collapse onto a single pair of master curves. We thus independently scale both the moduli and the frequency of each data set by factors  $a = 1/\omega_{cl}$  and  $b = 1/G_{cl}$ , respectively, as shown in figure 4.5 .

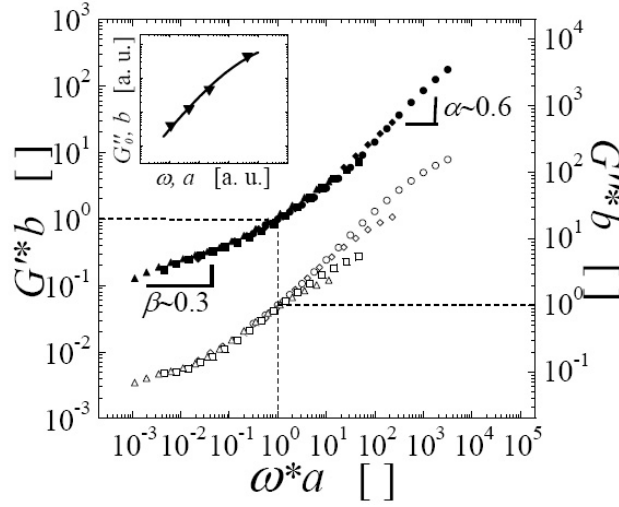


Figure 4.5: Master curves showing the elastic (full symbols, left axis) and viscous (empty symbols, right axis) scaled moduli for  $\phi \geq 3.4\%$ . Symbols are the same of figure 4.4. The inset shows the common scaling of the functions  $b = b(a)$  (reverse triangles) and  $G''_o = G''_o(\omega)$  of the neat polymer (solid line).

The scaled moduli lie on top of each other over more than six decades in frequency, corroborating the simple physical picture proposed. The analysis of the shift factors further supports the two-component model since the elasticity of the hybrids at the crossover, which is given by the relationship between  $b$  and  $a$ , shown in figure 4.5 scales along the viscous modulus of the background polymer,  $G''_0 = G''(\omega)$ . For  $\omega \cdot a \gtrsim 10$ , there are deviations of  $G''$  from the master curve; this is a direct consequence of the viscoelastic response of the polymer matrix, which dominates the high-frequency viscoelastic properties of the PNS and whose relaxation time is independent of filler content. The overall scaling supports the approach by Trappe and Weitz, emphasizing the separability of the particle structure and suspending medium dynamics, and the additivity of the elasticity of the two phases; in our system, this could be a direct consequence of the small polymer-filler in-

teraction. The scaling of figure 4.5 greatly clarifies the frequency dependence of the hybrid elasticity. Two different relaxation dynamics are evident, for  $\omega \cdot a$  greater and smaller than 1. For  $\omega \cdot a > 1$ , the elastic modulus approximately scales as  $G' \sim \omega^{0.6}$ . According to our simple two-component model, such dependence must reflect the storage component of the suspending polymer with the solid network in it. As will be shown in the next chapter, at these high frequencies hydrodynamic interactions between the two phases must be taken into account to explain the observed value of the exponent [12]. For  $\omega \cdot a < 1$ , the polymer contribution to the elasticity becomes unimportant and the relaxation kinetics of the cluster network emerges. The scaling emphasizes that the filler relaxation mechanism is the same for all volume fractions, provided  $\phi \geq 3.4\%$ . In contrast to permanent solidlike networks, which are characterized by a frequency independent elastic modulus, we find that  $G'$  scales with frequency as a power-law:  $G' \sim \omega^{0.3}$ ; this emphasizes the transient character of the cluster network, which must suffer from cluster rearrangements. Interestingly, this slow dynamic is reminiscent of colloidal glasses [19, 20] and has been observed in many other soft materials [21].

To further inquire about this analogy, we perform stress relaxation experiments to access the dynamics of our PNS at longer times. The measured time dependence of the relaxation modulus is shown in the inset of figure 4.3 and the results for the Fourier transformed moduli are plotted, as lines, in figure 4.3. There is excellent agreement between these results and the moduli directly determined in oscillatory tests, emphasizing the robustness of our experiments. Remarkably, the stress relaxation results reveal the existence of an ultimate relaxation time,  $\tau_r = 1/\omega_r$ , that we identify with the third crossover of  $G'$  and  $G''$  at very low frequencies (see figure 4.3). This final characteristic time is  $\phi$ -dependent, as shown in the extended scaling curve of  $G'$  (figure 4.6). The observation of this long-time relaxation suggests that above  $\phi_c$ , the percolating network of aggregates is strong enough to bear the applied stress, but still weak enough to allow rearrangements at sufficiently long times; the cluster network is thus transient in this sense. As  $\phi$  increases, the mobility of each network-building cluster is slowed down by the increased number of surrounding clusters, setting the time-scale for the macroscopic relaxation. Such idea is consistent with that of Segrè et al. [22], which states that the gel transition is a consequence of the arrest of clusters in cages of neighboring clusters, underlining the similarities between gel and glass transitions.

For times shorter with respect to the structural relaxation time of the network, the elasticity of our hybrids can be described with the notion of a percolating network. Shih et al. developed a scaling theory based on a fractal gel model to describe the  $\phi$ -dependence of both the elastic modulus and the critical strain separating the linear and non-linear regions [23]. The model predicts power-law dependences of the form  $G' \sim \phi^x, \gamma_c \sim \phi^y$  where

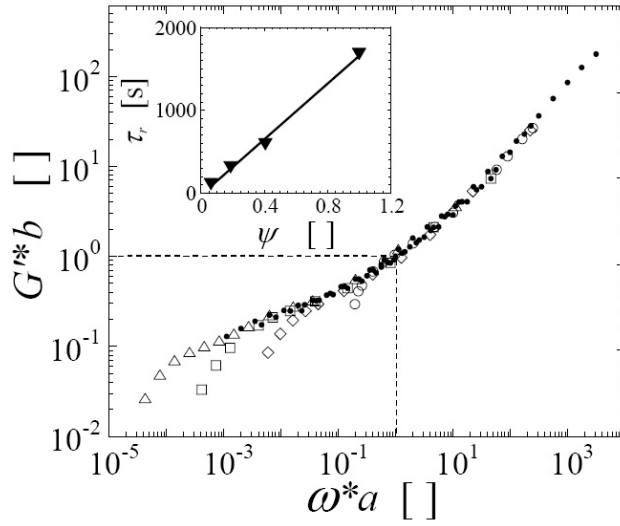


Figure 4.6: Extended master curve showing the scaled elastic moduli of the samples at  $\phi \geq 3.4\%$  as obtained by means of oscillatory scans (full circles) and Fourier transformation of the stress relaxation moduli,  $G(t)$  (empty symbols). Symbols are the same of figure 4.4. The inset shows the increase of the ultimate relaxation time  $\tau_r$  with the reduced volume fraction  $\psi = \phi/\phi_c - 1$  ( $\phi_c = 3.2\%$ ).

$x$  and  $y$  depend on the fractal dimension of the structures being formed. This model successfully describes several experimental data for flocculated suspensions [23]. More recent developments of fractal gel models predict different values of the exponents [24]. Close to the percolation threshold, alternative models describe the mechanical properties of the structure in terms of well-defined transition points, such as the  $\phi_c$  found for our PNS [12, 25]. These models propose power-law scalings of the form  $G' \sim (\phi/\phi_c - 1)^\nu$  and  $\gamma_c \sim (\phi/\phi_c - 1)^{-\lambda}$ , which characterize the approach to  $\phi_c$  and rigorously hold only in the vicinity of the percolation boundary [14].

Since our results are near the percolation threshold, we follow the percolation approach and critically test the previous hypothesis pertaining the existence of a percolation threshold around  $\phi = 3.4\%$ . We thus plot the cross-over elastic modulus  $G_{cl}$  and the critical strain  $\gamma_c$  as a function of the reduced volume fraction,  $\psi = \phi/\phi_c - 1$ . By adjusting  $\phi_c$  to 3.2%, we find power-law scalings for both variables, with  $\nu=1.7$  and  $\lambda=0.43$ , as shown in figure 4.7; this supports the idea of rigidity percolation occurring at  $\phi_c$ . The values of our exponents are in good agreement with those reported for three-dimensional systems characterized by a stress-bearing network with bond-stretching mechanisms [26, 27]. In particular, the value of  $\nu$  is close to the value reported by Rueb and Zukoski for octadecyl silica gels in Newtonian liquids,  $nu=(2.0 \pm 0.3)$  [25].

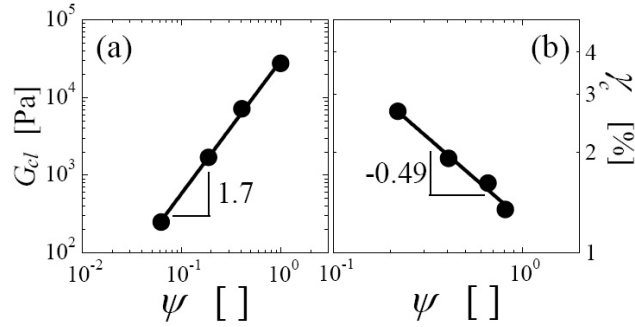


Figure 4.7: Critical behavior of the hybrid elasticity,  $G_{cl}$ , and critical strain,  $\gamma_c$ , for the samples at  $\phi \geq 3.4\%$ . Data are plotted against the reduced volume fraction  $\psi = \phi/\phi_c - 1$  ( $\phi_c=3.2\%$ ).

Finally, we emphasize that the characteristic time for the long-time structural relaxation,  $\tau_r$ , increases linearly with  $\psi$ , with  $\phi_c=3.2\%$  (inset figure 4.6). Similar qualitative behavior has also been observed in many different systems, including hard-sphere colloidal glasses [28] and depletion flocculated colloidal gels, both at high [29] and low [22, 17] concentrations. In all cases, the structural relaxation time is found to increase with particle volume fraction or attraction strength, reflecting the increased difficulty for

cluster cage breakup. Remarkably, in these systems, the increase of  $\tau_r$  with  $\phi$  is more pronounced when compared to what we have found. Further work must aim at elucidating the origin of this difference.

### 4.3 Conclusions

We have successfully extended the framework to understand the rheology of colloidal particle gels in Newtonian liquids to a polymer nanocomposite system with small polymer-particle interactions. Despite the apparent complex behavior of the frequency dependent moduli with filler concentration, the viscoelasticity of the system can be scaled onto a single pair of master curves over eight frequency decades reflecting the separation of the various time scales that characterize PNS; this is achieved above a critical volume fraction,  $\phi_c$ , which establishes the boundary for percolation of the filler. The space-spanning structure that results from this percolation exhibits a final relaxation at long times that depends on particle volume fraction and that is approached by a slow dynamic process. This reflects the transient character of the network and suggests that gelation could result from crowding of clusters, emphasizing the similarity between the gel and the glass transition: while the latter is driven by kinetic arrest of single particles, the gel arises from crowding and consequent arrest of clusters. Overall, the proposed analysis is expected to be useful to understand a wide variety of complex fluids in which a superposition of the elasticity of the components is possible. In particular, the elastic modulus has recently been suggested to follow a universal behavior with volume fraction also in case of polymer bridging mechanisms [30]. As a consequence, this would allow a separation of the contributions to the total elasticity following the present analysis. The generalization of our approach to such systems and other technologically relevant PNS, such as polymer-layered silicate nanocomposites still remains to be proved.

Chapter 4

# Bibliography

- [1] J. R. S. Warring, *Trans. Inst. Rubber Ind.* 26, 4 (1950); W. P. Fletcher, A. N. Gent, *Trans. Inst. Rubber Ind.* 29, 266 (1953)
- [2] Solomon M.J., Almusallam A.S., Seefeldt K.F., Somwangthanaroj A., Varadan P. *Macromolecules* 34, 1864 (2001)
- [3] Ren J., Silva A.S., Krishnamoorti R., *Macromolecules* 33, 3739 (2000)
- [4] R. Inoubli, S. Dagrou, A. Lapp, L. Billon, J. Peyrelasse, *Langmuir* 22, 6683 (2006)
- [5] Q. Zhang, L. A. Archer, *Langmuir* 18, 10435 (2002)
- [6] F. Saint-Michel, F. Pignon, A. Magnin, *J. Colloid Interface Sci.* 267, 347 (2003)
- [7] A. I. Leonov, *J. Rheol.* 34, 1039 (1990); P. Doremus, J. M. Piau, *J. Non-Newtonian Fluid Mech.* 39, 335 (1991)
- [8] P. N. Puesy PN and W. van Megen, *Nature* 320, 340 (1986); P. N. Puesy PN and W. van Megen, *Pys Rev Lett* 59, 2083 (1986)
- [9] A. H. Krall and D. A. Weitz, *Phys Rev Lett* 82, 1064 (1998); A. H. Krall, Z. Huang, D. A. Weitz, *Physica A* 235, 19 (1997)
- [10] V. Trappe, V. Prasad, L. Cipelletti, P. N. Segr, and D. A. Weitz, *Nature* 411, 772 (2001)
- [11] L. Cipelletti, S. Manley, R. C. Ball, and D. A. Weitz, *Phys. Rev. Lett.* 84, 2275 (2000)
- [12] V. Trappe and D. A. Weitz, *Phys. Rev. Lett.* 85, 449 (2000)
- [13] Y. Kantor and I. Webman, *Phys. Rev. Lett.* 52, 1891 (1984)
- [14] Stauffer D. and Aharony A., *Introduction to Percolation Theory* 2nd ed., Taylor & Francis, London, (1992)

Chapter 4

- [15] Russel, W. B.; Saville, D. A. and Showalter, W. R. *Colloidal dispersions* Cambridge university press 1989
- [16] Vermant J., Ceccia S., Dolgovskij M.K., Maffettone P.L., Macosko C.W. *J Rheol* 51, 429 (2007)
- [17] Prasad V., Trappe V., Dinsmore A.D., Segrè P.N., Cipelletti L., Weitz D.A. *Faraday Discuss* 123,1 (2003)
- [18] Wolthers W., Van den Ende D., Breedveld V., Duits MGH, Potanin AA, Wientjens RHW, Mellema J. *Phys Rev E* 56, 5726 (1997)
- [19] Shikata T. and Pearson D.S. *J Rheol* 38, 601 (1994)
- [20] Mason T.G., Weitz D.A. (1995) *Phys Rev Lett* 75, 2773 (1995)
- [21] Sollich P., Lequeux F., Hbraud P., Cates M.E. *Phys Rev Lett* 78, 2020 (1997)
- [22] P.N. Segrè, S.P. Meeker, P.N. Pusey and W. C. K. Poon, *Phys Rev Lett* 75, 958 (1995)
- [23] Shih W.H., Shih W.Y., Kim S.I., Liu J., Aksay I.A. *Phys Rev A* 42, 4772 (1990)
- [24] Wu H. and Morbidelli M. *Langmuir* 17, 1030 (2001)
- [25]
- [26] Arbabi S. and Sahimi M. *Phys Rev Lett* 47, 695 (1993)
- [27] Plischke M., Vernon D.C., Jos B., Zhou Z. *Phys Rev E* 60, 3129 (1999)
- [28] van Megen W., Underwood S.M. *Phys Rev E* 49, 4206 (1994)
- [29] Shah S.A., Chen Y.L., Schweizer K.S., Zukoski F. *J Chem Phys* 119, 8747 (2003)
- [30] Surve M, Pryamitsyn V, Ganesan V *Phys Rev Lett* 96,17780 (2006)

## Chapter 5

# Refinement of the scaling: PS-SiO<sub>2</sub> hybrids

### 5.1 Introduction

A way to enhance the mechanical, thermal and physical properties of polymers is to fill them with inorganic particles. Since such improvements depend on the interfacial properties between phases, the importance of using nanoparticles to increase the total surface area is easily understood. A direct consequence of incorporating nanoparticles in polymer melts is a profound change in the viscoelastic properties of the resulting nanocomposite. Such a change is the result of inter-phases interactions and of micro and meso-structures formation in the hybrid material. In particular, attractive colloidal particles are well known to form gels in simple liquids. Such gels are generally fractal networks that build up as the result of particle aggregation. Nevertheless, when the suspending liquid is a polymer, other networks of different nature may be formed. For example if the particles are close enough, a polymer chain may adsorb on the surfaces of the two particles forming a bridge between them. In this case a polymer-particle gel is formed. Among different additives, fumed silica is a widely used filler in polymer industry, made of primary particles of few nanometers fused together in aggregates whose dimensions span from tens to hundreds of nanometers. If the surface of the clusters is not organo-modified, attractive inter-particle forces are important when the particles are dispersed in a polymer melt. Then, if the viscosity of the suspending medium is low enough, Brownian motion of the clusters becomes relevant and leads to formation of agglomerates which eventually self-assemble to form a whole space spanning network of particles. Depending on the nature inter-phase affinity, either particle-particle or polymer-particle gels may be formed. In any case, since the network may bear stress, its main consequence on linear rheology is reflected in the appearance of a low frequency plateau of the elastic modulus  $G'$ . On the

contrary, inter-particle steric repulsion is induced by organo-modifying the particle surface. This reduces formation of agglomerates and the effect of the particles on the rheological response of the hybrid is weaker.

Although a wide literature exists, dealing with the linear viscoelastic moduli of polymer-nanoparticle hybrids, general physical models that allow interpreting their frequency response as function of volume fraction and type of interaction are still scarce. Such models are the key relating the structure to the final macroscopic properties of the material. A two-component model has been proposed in the previous chapter to describe the frequency dependence of the linear moduli of polymer-nanoparticle hybrids, when the enthalpic interactions between polymer and particles are negligible. The underlying physics of the model lies on the independent rheological responses of the polymer and the particle network. Then, for times longer than the polymer relaxation time, the only contribution to  $G'$  comes from the network. This elastic contribution depends on volume fraction  $\phi$  and scales along the matrix viscosity allowing for a universal scaling of the frequency dependent moduli measured at different  $\phi$ . Although the scaling works well, there are still unresolved issues regarding the interpretation and correctness of the values used to scale the curves. In this chapter the approach is extended to describe the frequency and particle volume fraction dependences of the viscoelastic moduli of a model nanocomposite system made of silica nanoparticles dispersed in a polystyrene (PS) matrix. This system is characterized by negligible polymer particle interactions. Once hydrodynamic contributions are removed, the physical meaning of the two-component model gets evident. This is reflected in the excellent scaling of the  $G'$  curves of samples at different  $\phi$ . The scaling, in turn, allows estimating the elasticity of networks which are too tenuous to be appreciated by a viscoelastic measurement. The analysis of the scaling factors allows investigating accurately the structure and elasticity of the particle network. We do this using both the percolation and fractal approaches, underlying the difficulties to get reliable values for the critical parameters.

## 5.2 Results

The hybrids are prepared by extruding a polystyrene with molecular weight  $M_w=125$  KDa and the silica ( $\text{SiO}_2$ ) nanoparticles with the procedure described in chapter 2. Due to their large specific surface area, colloidal fumed silica particles typically form stable aggregates during the fabrication process. The quenched internal morphology of two hybrids at particle volume fractions  $\phi=0.025$  and  $\phi=0.045$  soon after the extrusion process is shown in the TEM micrographs of figure 5.1.

In both samples, aggregates of a few hundred nanometers appear well distributed on microscale. Such a mesostructure, resulting from the shear

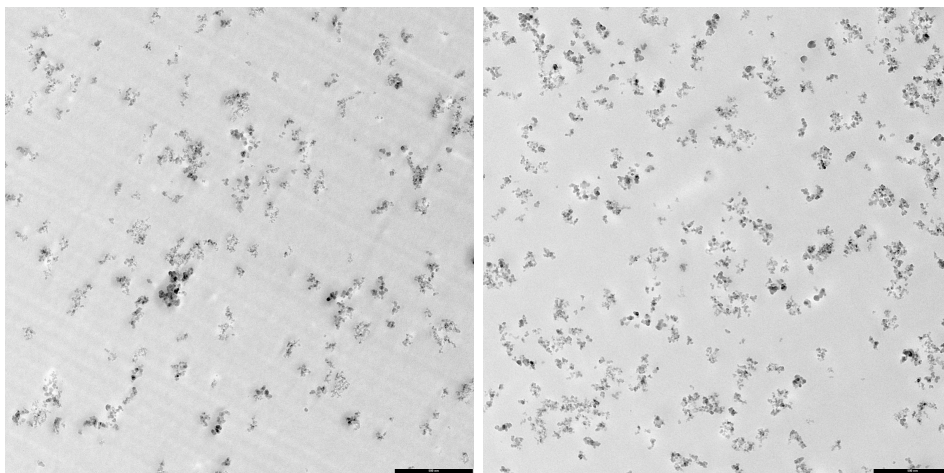


Figure 5.1: Tem micrographs representing the quenched microstructure of PS/SiO<sub>2</sub> samples after extrusion. Volume fractions are:  $\phi=0.017$  (left) and  $\phi=0.035$  (right). The scale-bar is 500 nm.

and elongational stresses experienced by the materials during extrusion, is far from equilibrium and the clusters are favorable to self-aggregation. In aggregating Newtonian colloidal dispersions, a growth during time of the linear viscoelastic moduli is generally observed, reflecting the rearrangements of the particles. Above a critical filler volume threshold, this leads to formation of a whole space-spanning network of particles [1, 2]. A similar behavior has been reported for polymer-based nanocomposites above the matrix melting or glass transition temperature [3, 4, 5]. Following previous arguments, we monitor the clustering in our systems by measuring the temporal evolutions of  $G'$  and  $G''$  during an oscillatory shear in the linear regime at  $\omega=0.05 \text{ rad/s}$ . Since at this frequency the polymer can be considered fully relaxed, the structural rearrangements of the solid phase are monitored. The results at 200 °C are plotted in figure 5.2 for hybrids at different compositions.

The elastic modulus increases during time at all volume fractions, the rate of growth progressively decreasing up to the reaching of a time-independent value. This ageing effect reflects the flocculation of the SiO<sub>2</sub> aggregates formed during extrusion, as shown in the TEM micrographs in figure 5.3 taken upon the samples at  $\phi=0.025$  and  $\phi=0.045$  after 4-hours ageing at 200 °C. In both samples the pristine aggregates assemble to form bigger, stringy-shaped structures. The formation of a percolating filler network, however, can be only guessed from the visual inspection of figure 5.3 due to the intrinsic two-dimensional feature of TEM micrographs.

To address the effect of nanoparticle concentration over the viscoelas-

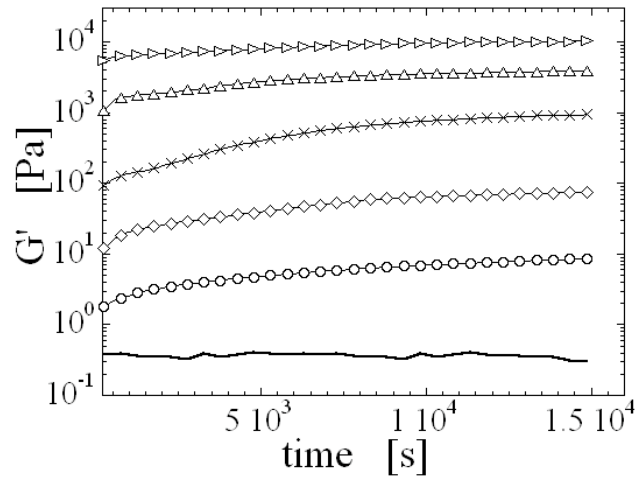


Figure 5.2: Time dependence of the linear viscoelastic moduli measured at  $\omega=0.05 \text{ rad/s}$  for PS/SiO<sub>2</sub> at volume fractions  $\phi= 0.01$  (circles), 0.017 (diamonds), 0.022 (crosses), 0.028 (triangles), 0.035 (arrows). The solid line is the neat PS

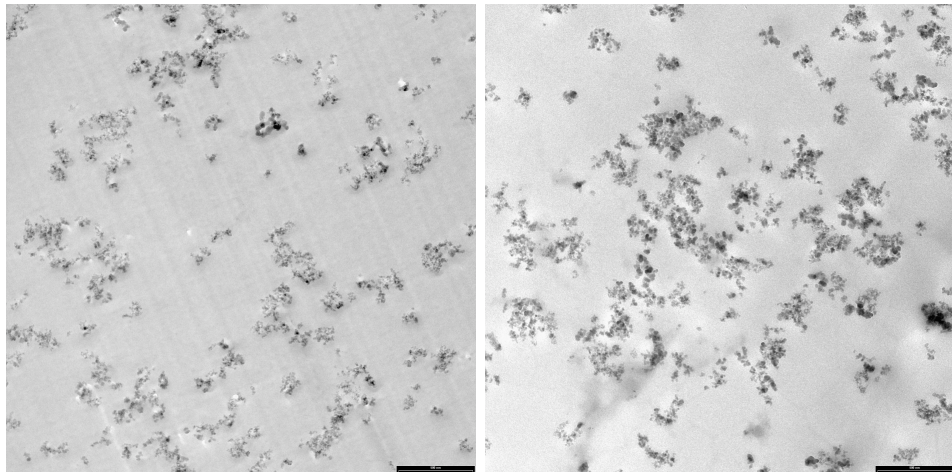


Figure 5.3: Tem micrographs representing the microstructure of PS/SiO<sub>2</sub> samples after 4 hours at 200 °C in quiescent state. Volume fractions are:  $\phi=0.017$  (left) and  $\phi=0.035$  (right). The scale-bar is 500 nm.

ticity of the hybrids we measure  $G'(\omega)$  and  $G''(\omega)$  as a function of  $\phi$  for  $0 \leq \phi \leq 0.041$  and plot the results in figure 5.4. The pure PS is predominantly viscous, with the loss modulus higher than the elastic one throughout the investigated frequency range.

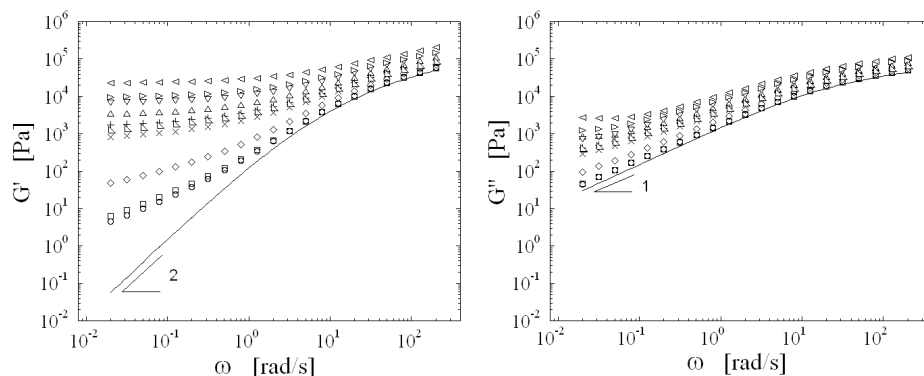


Figure 5.4: Frequency dependence of the elastic (left) and viscous (right) moduli at volume fractions  $\phi = 0.01$  (circles),  $0.013$  (squares),  $0.017$  (diamonds),  $0.022$  (crosses),  $0.023$  (half squares),  $0.025$  (plus),  $0.028$  (triangles),  $0.03$  (inverse triangles),  $0.035$  (right arrows),  $0.041$  (left arrows)

It exhibits viscoelastic Maxwellian behavior ( $G' \sim \omega^2$ ,  $G'' \sim \omega^1$ ) at low  $\omega$ . Both moduli of the hybrids increase monotonically with increasing filler loading in the whole frequency range. The faster relaxation modes of the hybrids, however, are essentially those of the unfilled polymer, the filler only causing a mere vertical shift of the curves for  $\omega \gtrsim 10^1 \text{ rad/s}$ . Gleissle and Hochstein accounted for a similar behavior in non-Newtonian melts filled with micron sized particles by introducing the concept of shear stress equivalent deformation [6]: the rigid particles reduce the effective gap distance available for the suspending medium by an amount proportional to the filler content. As a consequence, the inner shear amplitude experienced by the polymer is higher than the externally imposed, and the measured complex modulus,  $G^*$ , increases at all frequencies by the same factor  $B(\phi)$ . We argue that a similar hydrodynamic effect holds also for our nanohybrids in the high frequency region. Over longer timescales, however, the polymer matrix is relaxed and the filler significantly alters the viscoelastic response. In this regime, both  $G'$  and  $G''$  exhibit diminished frequency-dependences when compared to the PS. Such deviations indicate the occurrence of non-hydrodynamic stress contributions. The filler mainly affects the storage modulus, which exhibits a clear plateau  $G_o(\phi)$  at low  $\omega$  for  $\phi \geq 0.022$ . Taking into account the negligible polymer-particle interactions, this truly solid-like behavior supports the idea of an elastic, whole-space spanning network of

particles above a critical volume fraction,  $\phi_c$ . Interspersed throughout this structure is the suspending polymer phase, whose intrinsic viscoelastic feature mixes with the network dynamics giving rise to the complex frequency and volume fraction dependencies shown in figure 5.4. As a consequence of the different relaxation timescales, however, the rheological properties of the hybrids at  $\phi \geq \phi_c$  can be rationalized with a simple two-component model, first proposed for colloidal gels in Newtonian matrices, which combines the elasticity of the particle network and the viscosity of the suspending liquid [7, 8]. Following this approach, the elastic modulus is expected to scale with  $\phi$  along the viscosity of the neat matrix as a result of the increase of the network elasticity with filler content. We have recently shown that the two-component model allows describing the elasticity and dynamics of titanium dioxide nanoparticle gels in a polypropylene melt [9]. By normalizing the moduli of the hybrids at  $\phi > \phi_c$  with respect to the gel elasticity the curves collapse onto a single pair of master curves, validating the model.

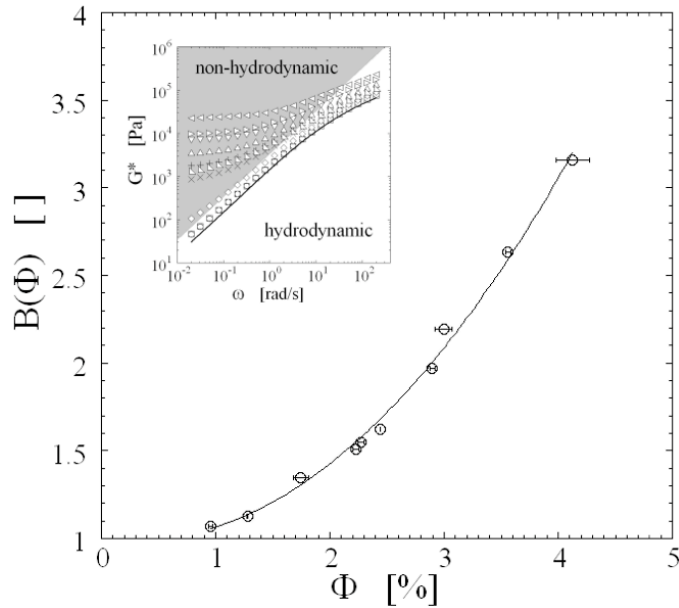


Figure 5.5: Volume fraction dependence of the hydrodynamic factor  $B(\phi)$ . The inset shows the frequency dependence of the complex modulus  $G^*$ . The  $\omega$  at which non-hydrodynamic effects become relevant increases with  $\phi$ . The sub-division in the hydrodynamic and non-hydrodynamic regions is hand-made to show the concept.

Till now, however, hydrodynamics effects have not been taken into account in the scaling procedure, and the curves have been scaled with respect to the low-frequency crossover between  $G'$  and  $G''$  of the hybrids [10]. Such

criterion does not reflect exactly the physical meaning of the model, in which the elasticity of the filler network should be scaled along the merely  $\omega$  dependent loss modulus of the neat matrix, once hydrodynamics effects related to the presence of the solid phase have been taken into account. Using the approach of Gleissle and Hochstein we evaluate  $B(\phi)$  as  $B(\phi) = G^*(\phi)/G_{PS}^*$  in the hydrodynamic region (inset of figure 5.5), which is reported in figure 5.5. Once amplified the loss modulus of the neat polymer by  $B(\phi)$ , we identify the horizontal ( $a$ ) and vertical ( $b$ ) shift factors to build the master curve of  $G'$  as the points where the particle gel elasticity,  $G_o(\phi)$ , equals the viscous component of the matrix corrected for the hydrodynamic effects,  $B(\phi) \cdot G_{PS}''$ . An example of how  $a$  and  $b$  are obtained for the hybrid at  $\phi=0.028$  is shown in the inset of figure 5.6.

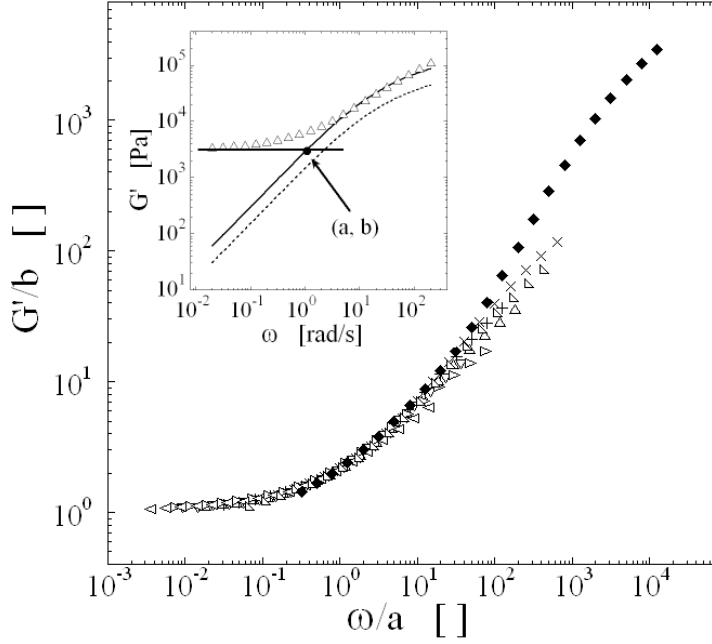


Figure 5.6: Master-curve of the elastic modulus obtained by scaling the  $G'$  curves of the hybrids at  $\phi > \phi_c$  (open symbols). The procedure through which the scaling factors  $a$  and  $b$  are obtained is shown in the inset for a sample at  $\phi=0.028$  and discussed in the text. The frequency dependence of the elastic moduli reported in the inset are for: the hybrid at  $\phi=0.028$  (triangles), neat PS (dashed line) and the neat PS multiplied by  $B(\phi = 0.028)$  (solid line). Solid points in the main figure is the curve for the sample at  $\phi=0.017$ , shifted to obtain the best collapse on the master-curve.

We test the validity of our approach by scaling the  $G'$  curves of the hybrids at  $\phi \geq 0.022$ , in which the existence of the particle network can be argued from the presence of a clear low-frequency plateau. The resulting master curve shown in figure 5.6 (open symbols) supports the approach adopted: the scaled moduli lie on top of each other in the low-scaled frequency range, while deviations emerge for  $\omega/a$  greater than  $\simeq 10^1$ . This is not unexpected, however, as it stems from the viscoelastic feature of the polymer matrix, dominating the high-frequency behavior and whose relaxation time is not scalable since it is independent on  $\phi$ .

The master curve demonstrates that the contributions to the hybrids elasticity of filler network and polymer matrix can be separated due to their different temporal relaxation scales. The two-component model, however, only applies for samples with filler volume fractions  $\phi$  greater than a critical value  $\phi_c$ , representing the minimum volume fraction necessary for the formation of an elastic stress-bearing network. Detecting such percolation threshold represents a critical issue, and many different approaches can be used.

The liquid-solid transition for suspensions in which the filler particles aggregate into sample spanning complexes share the same features of chemical gelation, namely the divergence of the longest relaxation time, and a power law spectrum [11]. Using sol-gel arguments, Inoubli et al. estimated  $\phi_c \simeq 0.025$  for polybutylacrylate-silica nanocomposites [12]; similarly, Casagnau found  $\phi_c \simeq 0.033$  for ethylene vinyl acetate copolymer-silica hybrids [13]. Using light scattering methods, Piau et al. estimated  $\phi_c \simeq 0.01$  for silica-silicone gels [14].

On the other hand, percolation theories predict the elastic modulus of the particle network near the percolation threshold to grow in a critical fashion with  $\phi$ ,  $G_o \sim (\phi - \phi_c)^\nu$  [15] suggesting a simple way to estimate  $\phi_c$ . Following this approach, the vertical shift factors  $b(\phi) = G_o(\phi)$  of the samples at  $\phi \geq 0.022$  were fitted to the equation

$$G_o = K \cdot (\phi - \phi_c)^\nu \quad (5.1)$$

in which  $K$  and  $\nu$  were set as fitting parameters and  $\phi_c$  was arbitrarily varied. The results of the fitting procedure are summarized in table 5.1 for different values of  $\phi_c$  and the corresponding fitting curves are shown in figure 5.7.

A weak dependence of the regression  $R^2$  on the value of  $\phi_c$  can be noticed, suggesting that a mere best fitting approach is not a reliable method for the detection of the percolation threshold. Instead, we use the following procedure: first, at each  $\phi_c$  we extrapolate the values of  $G_o$  for the hybrid at  $\phi=0.017$ , which are reported in table 5.1 as well. From figure 5.4 we estimate that the maximum acceptable value of  $G_o$  to be  $G_o(\phi = 0.017) \simeq 40Pa$ , which is the lowest value of  $G'$  experimentally accessible for this sample.

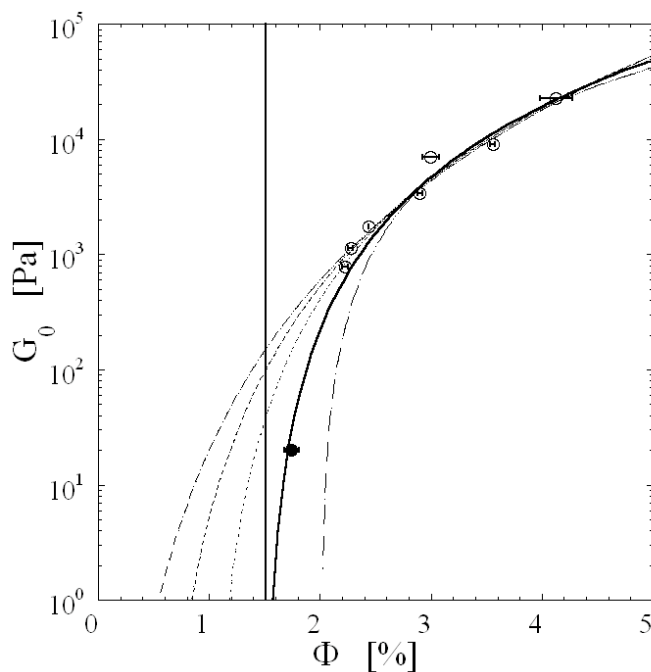


Figure 5.7: Volume fraction dependence of the network elasticity  $G_o$  (symbols). Open and solid symbols have the same meaning as in figure 5.6. Lines are fitting of the data to equation 5.1 varying  $\phi_c$ . From left to right  $\phi_c = 0, 0.5, 1, 1.5, 2$ .

$\phi_c$ [%]	$K$ [Pa]	$\nu$ [ ]	$R^2$ [ ]	$G_o(\phi = 0.017)$ [Pa]
0	20.2	4.9	0.9880	280
0.5	97	4.2	0.9875	215
1	413	3.5	0.9867	120
1.5	1527	2.8	0.9850	20
2	4670	2.0	0.9806	N.A.

Table 5.1: Fitting parameters to equation 5.1

Thus, by comparing the estimated value of  $G_o$  with the extrapolated ones we conclude that values  $\phi_c < 0.015$  must be discarded. On the other hand, we observe that  $R^2$  drops rapidly when passing from  $\phi_c=0.015$  to  $\phi_c=0.02$ . On the basis of previous observations we assert that  $\phi_c=0.015$  is the most reasonable value for the percolation threshold in this system, irrespective of the analysis of the  $R^2$  values. This value is also in agreement with that found by Pouchelon and Vondracek through rheological analyses [16], and the one inferred by Barthel from theoretical considerations [17]. Further support to the reliability of our estimation of  $\phi_c$  comes from the analysis of the master curve. Actually, an important consequence of the scaling shown in figure 5.6 is that the network elasticity can be estimated for all samples above  $\phi_c$  from the factor  $b$  required to scale the data. This allows determining  $G_o$  even for weak networks, whose modulus is too low to be measured directly through a simple frequency scan [10]. This is the case of the sample at  $\phi=0.017$ , which is above the estimated percolation threshold but whose plateau modulus cannot be inferred from the experimental data of figure 5.4. Shifting the curve of this sample on the master curve (solid symbols in figures 5.6, 5.7) allows estimating its elasticity. We observe that, once added to the data of figure 5.7, the extrapolated point (solid symbol) follows well the critical behavior previously found, supporting the validity of the procedure employed. The value of the critical percolation exponent  $\nu$  depends on the stress-bearing mechanism of the percolating filler network, and it ranges from  $\nu \simeq 2.1$  for systems in which the particles are free to rotate about each other, to  $\nu \simeq 3.75$  in the case of networks in which the chains can resist stress either by stretching or bending of single-bonds of the chain [18, 19]. For  $\phi_c=0.015$  we find  $\nu=2.8$ , in line with the result of Grant and Russell, who found a universal response with  $\nu = 3 \pm 0.5$  for suspensions of octadecyl silica particles irrespective of the strength of interparticle attraction [20]. Looking at the data of table 5.1, however, we stress the high sensitivity of the  $\nu$  on  $\phi_c$ , which makes hard to draw any conclusion about the actual stress bearing mechanism of the system. The particle network characterizing our systems at  $\phi > \phi_c$  is expected to exhibit scale invariance and can be described as a fractal structure. The mass of the network is therefore predicted to scale as  $L^D$ , where  $L$  is the size and  $D \leq 3$  is the Hausdorff or fractal dimension [21]. The value of  $D$  depends on the mechanism of particle assembling, ranging from  $D \simeq 1.75$  for diffusion-limited aggregation (DLA) to  $D \simeq 2.05$  for reaction-limited aggregation (RLA) [22]. The viscoelastic properties of aggregating colloids can be described using a fractal approach since the structure transmits stress through the chains of the elastic backbone. Modelling the colloidal gel as resulting from the aggregation of fractal flocs, Shih and co-workers have developed a scaling theory for a gel far from the gelation threshold for both the elastic modulus,  $G_o$ , and the maximum strain at which linear elastic behavior vanishes,  $\gamma_{cr}$  [23]. Provided that the links between the flocs are

stronger than those between the particles in the flocs, their model predicts that  $G_o \sim \phi^x$ , with  $x = (3 + b)/(3 - D)$ , and  $\gamma_{cr} \sim \phi^{-y}$ , with  $y = (1 + b)/(3 - D)$ . Here,  $b < D$  is the backbone fractal dimension, and it has values greater than unity in the case of spherical particles to provide a connected path.

To estimate the limit of linearity of the samples, the viscoelastic moduli are recorded at increasing oscillation amplitude  $\gamma$  at  $\omega = 0.05 \text{ rad/s}$ , that is a frequency low enough to consider the response of the hybrids governed by the particle network. We set the critical strain  $\gamma_{cr}$  for network breakdown as the point at which  $G'$  deviates of 5% from its constant low-strain value.  $G_o$  and  $\gamma_{cr}$  for the samples at  $\phi \geq 0.017$  are plotted as a function of  $\phi$  in figure 5.8.

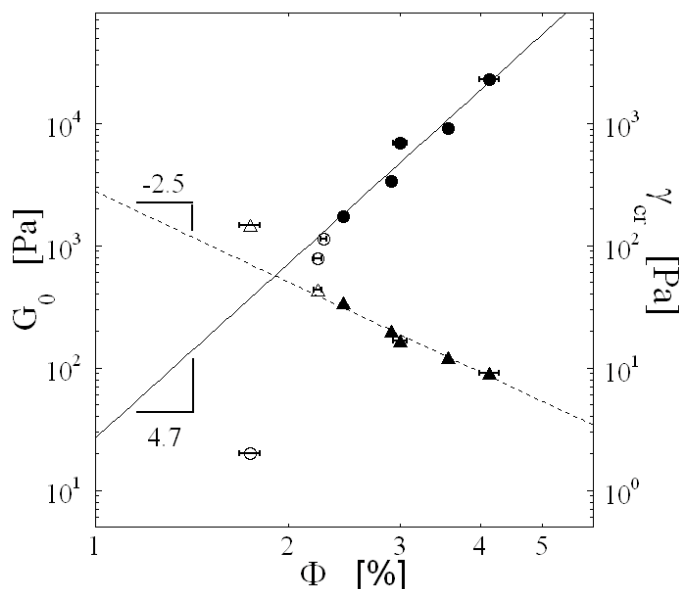


Figure 5.8: Volume fraction dependence of the network elasticity  $G_o$  (circles) and critical strain  $\gamma_{cr}$  (triangles). Solid symbols are considered far from the threshold and are fitted to the Shih's equations (solid and dashed line)

Fitting a power-law to the data at  $\phi \geq 0.024$  (solid symbols of figure 5.8) to fulfill the requirement of the Shih's model to be far from  $\phi_c$ , we get  $x = 4.7 \pm 0.3$  and  $y = 2.5 \pm 0.2$ . This leads to fractal dimensions  $D = 2.1 \pm 0.2$  and  $b = 1.3 \pm 0.2$ , in agreement with the results by Shih et al. for aqueous suspensions of bohemite alumina nanopowders. The value of  $D$ , is also in good agreement with the findings by Yzquier et al. [24] and Paquien et al. [25] for silica based suspensions. The experimentally deduced backbone fractal dimension  $b$  indicates a slightly tortuous connection path between

Chapter 5

the flocs, which appears in agreement with TEM investigations. However, as for the percolation exponents, we remark that the high variability of  $D$  and  $b$  make hard to drive any conclusion about the reliability of the Shih's model.

# Bibliography

- [1] Russel, W. B.; Saville, D. A. and Showalter, W. R. *Colloidal dispersions* Cambridge university press 1989
- [2] Cipelletti L., Manley S., Ball R.C. and Weitz D.A., Phys. Rev. Lett. 84, 2275 (2000)
- [3] Galgali G., Ramesh C. and Lele A., Macromoleciules 34, 852 (2001)
- [4] Reichert P, Hoffman B, Bock T, Thomann R, Millhaupt R and Friedrich C, Macromol. Rapid Commun. 22, 519 (2004)
- [5] Huang Y. Y., Ahir S. V., and Terentjev E. M., Phys. Rev. B 73, 125422 (2006)
- [6] Gleissle W. and Hochstein B., J Rheol 47, 897 (2003)
- [7] Trappe V. and Weitz D.A. Phys Rev Lett 85, 449 (2000)
- [8] Trappe V., Prasad V., Cipelletti L., Segr P.N., Weitz D.A. Nature 41, 772 (2001)
- [9] G. Romeo, G.Filippone, A. Fernandez-Nieves, P. Russo, and D. Acierno Rheol Acta (2008), DOI 10.1007/s00397-008-0291-2
- [10] Prasad V., Trappe V., Dinsmore A.D., Segr P.N., Cipelletti L., Weitz D.A. Faraday Discuss 123,1 (2003)
- [11] Winter H.H., Mours M. Adv Polym Sci134, 165 (1997)
- [12] Inoubli R., Dagreou S., Lapp A., Billon L., Peyrelasse J. Langmuir 22, 6683 (2006)
- [13] Cassagnau P. Polymer 44, 2455 (2003)
- [14] Piau J-M., Dorget M., Palierne J-F., J Rheol 43, 305 (1999)
- [15] Stauffer D. and Aharony A., *Introduction to Percolation Theory* 2nd ed., Taylor & Francis, London, (1992)

*Chapter 5*

---

- [16] A. Pouchelon, P. Vondracek, Rubber Chem. Technol. 62, 788 (1986).
- [17] H. Barthel, Colloids Surf. 101, 217 (1995)
- [18] Arbabi S. and Sahimi M. Phys Rev B 47,695 (1993)
- [19] Sahimi M. and Arbabi S., Phys Rev B 47, 703 (1993)
- [20] Grant M.C. and Russel W.B. Phys Rev E 47, 2606 (1993)
- [21] Weitz D.A. and Oliveira M. PRL 52,1433 (1984)
- [22] Weitz D.A., Huang J.S., Lin M.Y., Sung J., PRL 53,1416 (1985)
- [23] Shih W.H., Shih W.Y., Kim S.I., Liu J., Aksay I.A. Phys Rev A 42, 4772 (1990)
- [24] Yzquier F., Carreau P.G., Tanguy P.A., Rheol Acta 38, 14 (1999)
- [25] Paquien J.N., Galy J., Grard J.F., Pouchelon A. Colloid Surf A Physico-chem Eng Asp 260,165 (2005)

## Chapter 6

# Formation and yielding of the elastic network

### 6.1 Introduction

Polymer nanocomposites have attracted a great interest in the last decade because of their potential as technological materials, due to a dramatic increase of interfacial area and reduction of the wall to wall distance between fillers if compared to the relative microcomposites [1]. Melt state viscoelastic properties are strongly influenced by interface characteristics, particles size and shape and internal mesostructures [2, 3], making rheology a powerful and handling characterization technique of complex fluids. However, correlations between rheological parameters and microstructures is still ambiguous because of the complexity of these systems. The most successful rheological models [4] introduce various simplifying assumptions that are difficult to validate. The filler size effect on the overall material behaviour was attributed to either particle-particle [5, 6, 7] or polymer-particle [8, 9, 10] affinities. A shared feature of different nanocomposites, is the dramatic enhancement of the elastic modulus,  $G'$ , at low frequencies with respect to the hosting polymer, reflecting the presence of slow relaxation dynamics [8, 9, 10, 11]. Another feature, shared by many colloidal systems in general, is the growth of both storage and loss moduli during aging above the matrix melting temperature [8, 11, 12]. In colloidal systems and suspension literature [13, 14] this effect is generally addressed to cluster formation and, above a critical particles volume fraction,  $\phi_c$ , to the presence of a whole space spanning network of flocs. In this chapter I report the morphology and dynamics of a polypropylene filled with alumina nanospheres around the critical volume fraction. I show that particles aggregate in the melt, forming a three-dimensional network. This network is responsible for the liquid-like to solid-like transition of the nanohybrid. The application of large amplitude oscillatory shear progressively destroys the network leading to a

flow induced structure that cannot significantly contribute to the elasticity of the hybrid.

## 6.2 Results

$\text{Al}_2\text{O}_3$  nanoparticles are difficult to disperse in PP because of their large specific surface area and incompatibility in surface characteristics between their hydrophilic oxide surfaces and the hydrophobic non polar solvent [15]. The high stresses during extrusion, however, break the aggregates, reducing the clusters dimensions,  $D$ . The minimum cluster size depends on the applied stress and the composite Hamaker constant for two surfaces of a medium 1 interacting through a medium 2 [16]. The quenched internal morphology of the extruded hybrids at particle volume fraction,  $\phi$ , of 0.042 soon after the exit from the die is shown by TEM images in Figure 6.1 *a, b*.

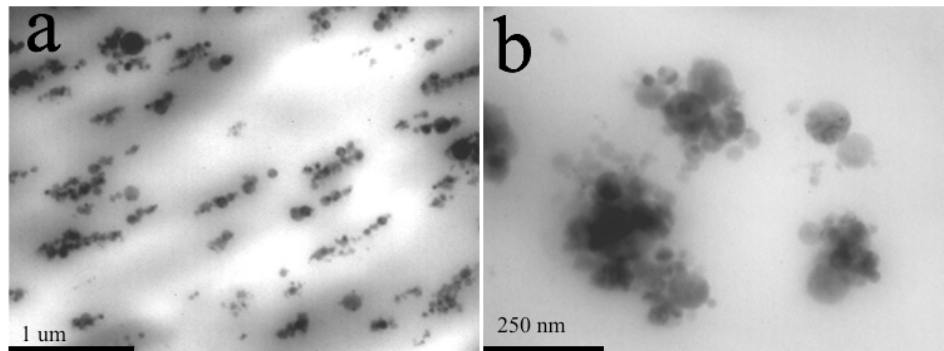


Figure 6.1: Tem micrographs showing the quenched microstructure resulting after extrusion for the hybrid at  $\phi= 0.042$ .

Although a homogeneous distribution can be observed on mesoscopic scale (figure 6.1 *a*), higher magnifications highlight the presence of aggregates of a few hundred nanometers (figure 6.1 *b*). The aggregates appear as open structures formed of tens of nanospheres of different sizes. These non-equilibrium structures rearrange towards a more favourable thermodynamic state during a subsequent aging above the PP melting temperature. The rearrangement was followed by observing the evolutions of the linear viscoelastic moduli during a low frequency (0,0628 rad/sec) time sweep test, as reported in 6.2 for two samples at different particle volume fractions.

The sample at  $\phi=0.026$  shows a weak increase of both moduli during the first seconds of test. Then, a stationary condition is reached with negligible changes during time. The system at  $\phi=0.042$  shows a very different behaviour: its elastic modulus drastically increases and a stationary final value, significantly higher than that at the beginning of annealing, is reached after

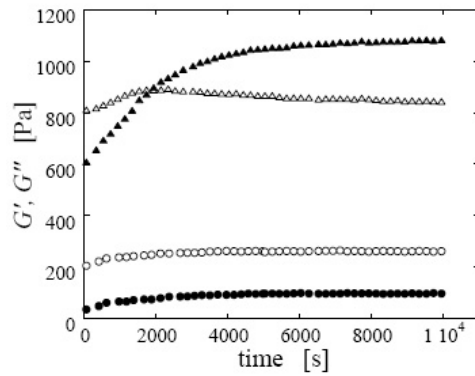


Figure 6.2: Time dependence of the elastic (solid symbols) and viscous (open symbols) moduli for PP-Al<sub>2</sub>O<sub>3</sub> hybrids at  $\phi=0.026$  (circles) and  $\phi= 0.042$  (triangles).

about 2000 seconds. Conversely, the viscous component remains almost constant during the test. This leads to a liquidlike to solidlike quasi-quiescent transition indicative of the inorganic phase structuring during time. Morphological rearrangements after a 3-hours annealing were visualized by TEM images on the solid samples at  $\phi=0.042$ . The microstructure was investigated by observing the same samples used during rheological investigations. The samples were cooled after rheological tests by using gaseous nitrogen, and the disks were removed from the plates of the rheometer and treated for morphological analyses. As reported in figure 6.3 the individual aggregates resulting from the extrusion form an interconnected network after annealing [17].

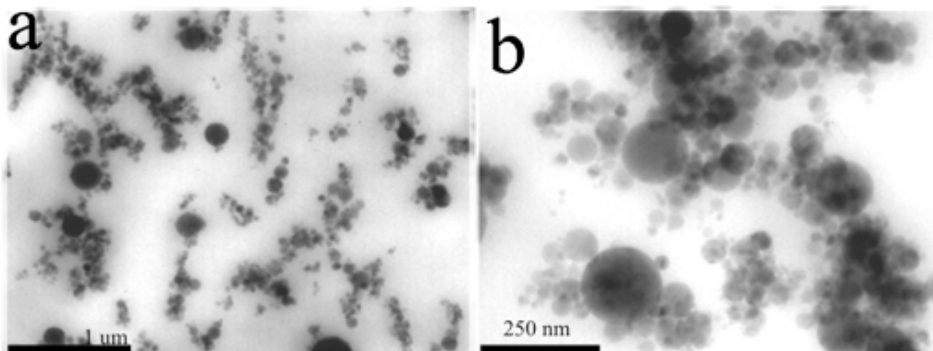


Figure 6.3: Tem micrographs showing the microstructure of the hybrid at  $\phi= 0.042$  after 3-hours aging at 190 °C.

This network can store the elastic energy of the applied deformation for times much longer than the neat polymer or non-structured hybrids, as shown in figure 6.4. The relaxation dynamics may be indifferently monitored by stress relaxation (figure 6.4 *a*) or frequency sweep tests (figure 6.4 *b, c*.)

In linear regime, these tests may be compared by Fourier transforming  $G(t)$ . For both the 3-hours aged samples at the two particle volume fractions, the Fourier transformed  $G'(\omega)$  and  $G''(\omega)$  agree well with the directly measured ones from oscillatory experiments as shown in figure 6.4 *b, c*). However, a step shear strain allows to monitor a longer time response than oscillatory experiments, because of limitation of the experimental time in the low frequency range. Moreover, typical experimental times in stress relaxation tests on extruded samples are no longer than 50 seconds, so that the changes of viscoelastic properties due to aging can be neglected. At frequencies higher than  $1 \text{ rad s}^{-1}$ , all materials share similar fast relaxation dynamics, related to relaxation of polymer molecules.

The low frequency responses of the 3-hours aged sample at  $\phi=0.026$  and as extruded sample at  $\phi=0.042$  are qualitatively similar to that of the neat PP, the hybrid full relaxation only occurring at times longer than the homopolymer ones. Differently, a new long time relaxation dynamic characterizes the behaviour of the sample at  $\phi=0.042$  after aging. A pseudo-solidlike behaviour is observed in the frequency range between  $10^{-2} \div 10^2 \text{ rad/s}$ , while the slowest dynamic (below  $10^{-2} \text{ rad/s}$ ) accounts for the Brownian relaxation of the filler network. The results shown suggest that a critical particle volume fraction around 0.04 exists for the studied PP- $\text{Al}_2\text{O}_3$  nanohybrids. In fact, little differences in volume fraction or state of dispersion determine very different rheological responses. It is well known that glasses and physical gels remain trapped in metastable configurations because the energy barriers associated to particles rearrangement are very large compared to thermal energies [2, 13, 18, 19].

Application of large strains after aging may provide an excess energy to overcome these barriers and the system evolves toward a different configuration. In figure 6.5,  $G(t)$  is reported after the application of large amplitude oscillatory shear (LAOS) for different deformation amplitudes on the 3-hours aged sample at  $\phi=0.042$ . LAOS was applied until the moduli reached a constant value in time (no more than 1000 seconds were needed in any case) at a frequency of  $0.0628 \text{ rad/s}$ . Subsequently, time sweep tests in linear regime were performed on the sample (inset in figure 6.5) in order to let the moduli stabilize before stress relaxation testing. Figure 6.5 clearly shows that each LAOS has a drastic effect on  $G(t)$ , the more the deformation amplitude, the faster the relaxation dynamics.

The morphology of the sample after the LAOS at  $\gamma=5$  is reported in 6.6. The network formed during aging is no more visible and the presence of many small clusters characterizes the sheared system. The analysis of TEM images allowed getting a cluster size cumulative distribution (CSD),

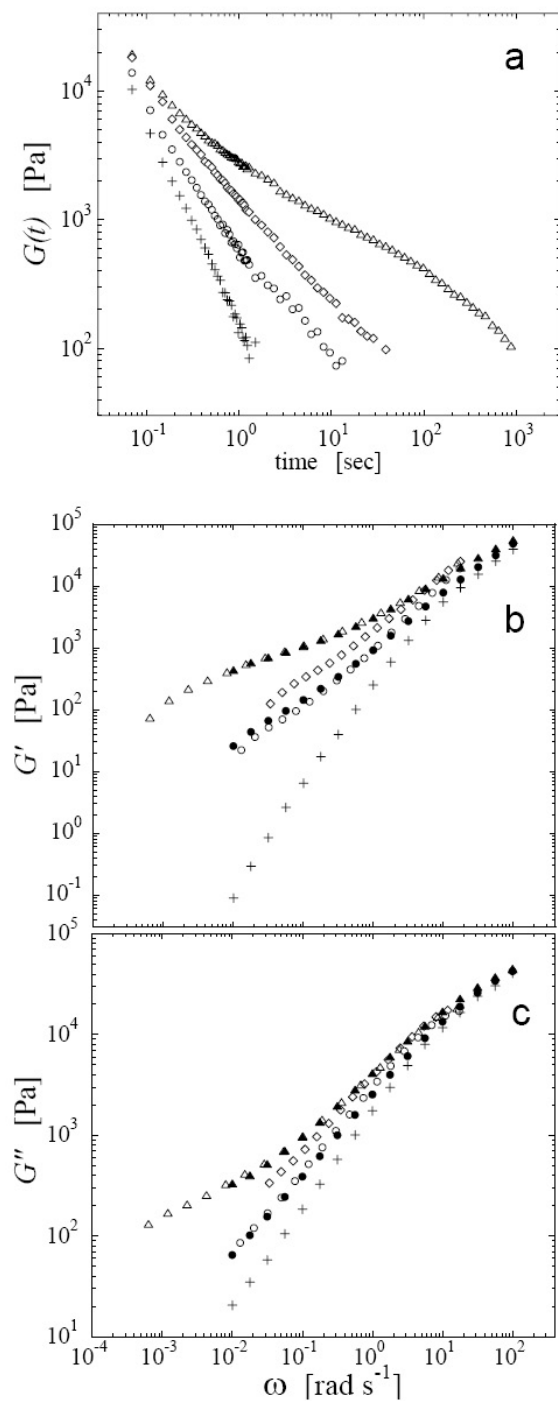


Figure 6.4: Stress relaxation moduli (a) and elastic (b) and viscous (c) moduli for: neat polypropylene (crosses), 3-hours aged hybrids at  $\phi=0.026$  (circles) and  $\phi=0.042$  (triangles). The as-extruded sample at  $\phi=0.042$  is also reported (diamonds). In b, c, solid symbols represent direct measurements from oscillatory test, while open symbols are the Fourier transformed dynamic moduli from stress relaxation data.

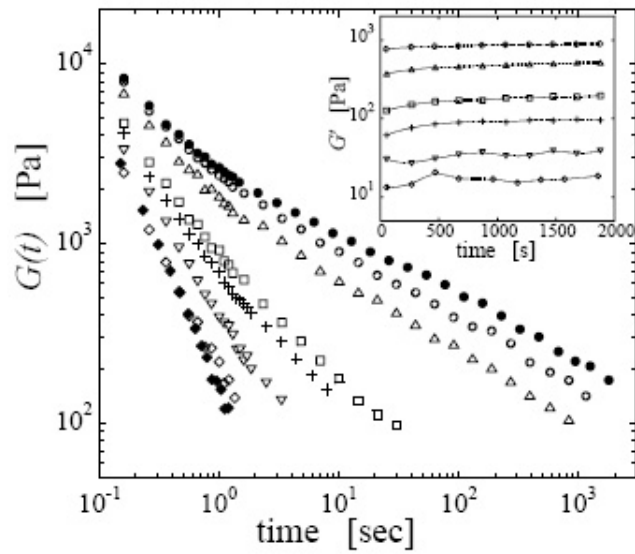


Figure 6.5: Relaxation moduli of the 3 hours annealed nanohybrid at  $\phi=0.045$  after oscillatory shear flows at strain amplitudes of 0.008 (solid circles), 0.1 (open circles), 0.25 (triangles), 0.5 (squares), 1 (crosses), 2.5 (reverse triangles), 5 (diamonds) and neat polymer (solid diamonds). The recovery during time of the linear elastic moduli after the large amplitude shear flows is shown in the inset. The symbols used are the same of the stress relaxation moduli.

reported in figure 6.7 for the as extruded, aged, and sheared after aging samples at  $\phi=0.042$ .

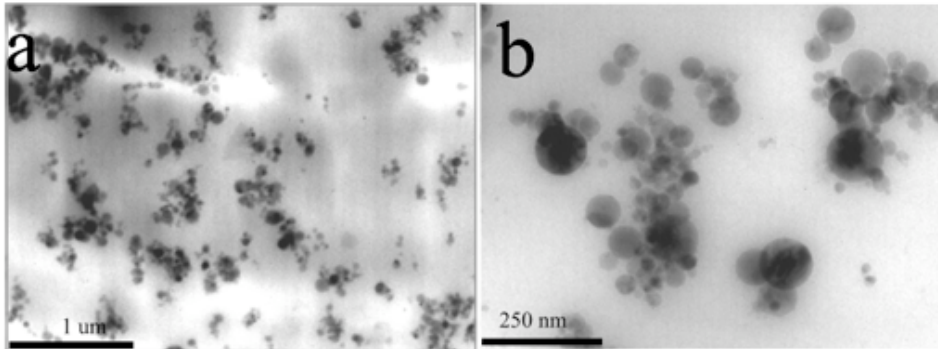


Figure 6.6: Morphology of the 3-hours annealed sample at  $\phi=0.042$  after the LAOS at  $\gamma=5$  as obtained from TEM

The analysis of TEM images allowed getting a cluster size cumulative distribution (CSD), reported in figure 6.7 for the as extruded, aged, and sheared after aging samples at  $\phi=0.042$ .

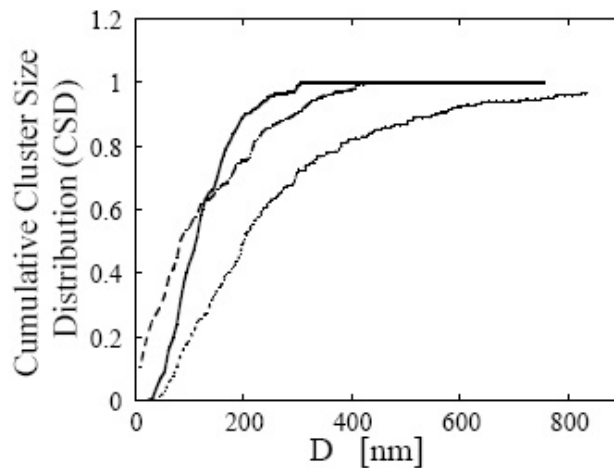


Figure 6.7: Cumulative cluster size distribution for the sample at  $\phi=0.042$ , as-extruded (solid line), the 3-hours annealed sample (dotted line), and three hours annealed after LAOS at  $\gamma=5$  (dashed line).

The CSD of the extruded sample is rather sharp, indicating the efficiency of the extrusion process. The effect of thermal annealing is a significant smoothing of the CSD, with the appearance of very large clusters. This

confirms the metastability of the samples, evolving toward states of less free energy under the push of the strong particle-particle interactions. Finally, the large deformation after the annealing strongly affects the sample microstructure: a relevant sharpening of the CSD can be observed, with the disappearance of the bigger clusters formed during the aging and the recovery of an as extruded-like microstructure. However, the presence of smaller aggregates characterizes the sheared system respect to the as extruded one. In summary, we have used a simple polymer-nanoparticles model system to describe many common features shared by nanocomposites and colloidal suspensions. The drastic increase of the rheological properties respect to the matrix in the studied systems characterized by poor polymer-particles interactions has been related to the formation of a network above a critical particles volume fraction, as a consequence of particles and clusters rearrangement. The elasticity of the network adds to that of the polymer, storing the stress induced by a deformation in linear regime for times much longer than those of the polymer molecules. The dynamics of this transient network are well observable in stress relaxation tests in which the long time decay of  $G(t)$  is addressed to the network Brownian relaxation. The application of large amplitude oscillatory shear provides an excess energy to the system to escape from the metastable configuration in which is trapped, destroying the network and leading to a flow-induced structure which can no more significantly contribute to the system elasticity.

# Bibliography

- [1] Friedrich, K.; Fakirov, S.; Zhang, Z. *Polymer composites: From nano-to macro-scale* Springer 2005; Krishnamoorti, R.; Vaia, R.A.; Giannelis, E.P. *Chem.Mater.* 1996, 8, 1728-1734
- [2] Larson, R.G. *The structure and rheology of complex fluids*; Oxford university press: New York 1999.
- [3] Barnes, H. A. *The rheology of filled viscoelastic systems: a review* in *Rheology Reviews* 2003, British Society of Rheology, 2003, ISBN 0-9538904-8-1, pp. 1-36 2003
- [4] Leonov, A. I. *J. Rheol.* 1990, 34, 1039. Doremus, P.; Piau, J. M. *J. Non-Newtonian Fluid Mech.* 1991, 39, 335
- [5] Ren, J.; Silva, A.S.; Krishnamoorti, R. *Macromolecules* 2000, 33, 3739-3746; Mitchell, C.A.; Krishnamoorti, R. *J. Polym. sci. B: polym. Phys.*, 2002, 40, 1434-1443.
- [6] Galgali, G.; Ramesh C.; Lele, A. *Macromolecules* 2001, 34, 852.
- [7] Cassagnau, Ph; Mlis, F. *Polymer* 2003, 44, 6607.
- [8] Zhang Q.; Archer L.A. *Langmuir* 2002, 18, 10435; Zhang, Q.; Archer L.A. *Macromolecules* 2004, 37, 1928-1936.
- [9] Vacatello, M. *Macromolecules* 2001, 34, 1946. Vacatello, M. *Macromol. Theory Simul.* 2002, 11, 757-765.
- [10] Sarvestani, A. S.; Picu, C. R. *Rheol Acta* 2005, 45, 132-141.
- [11] Krishnamoorti, R., Yurekly, K. *Curr. Opin. Colloid Interface Sci* 2001, 6, 464-470
- [12] Reichert P.; Hoffman B.; Bock T.; Thomann R.; Mulhaupt R.; Friedrich C. *Macromol Rapid Commun.* 2001, 22, 519.
- [13] Russel, W. B.; Saville, D. A. and Showalter, W. R. *Colloidal dispersions* Cambridge university press 1989

Chapter 6

- [14] Cipelletti, L.; Manley, S.; Ball, R. C.; Weitz, D. A. Phys. Rev. Lett. 2000, 84, 2275.
- [15] Liu, J; Jean, J.; Li, C. J. Am. Ceram. Soc. 2006, 89, 882-887.
- [16] Baird, D. G.; Collias, D.I. Polymer processing principles and design Butterworth-Heinemann 1995.
- [17] Trappe, V.; Weitz, D. A. Phys. Rev. Lett. 2000, 85, 449.
- [18] Götze, W. J. Phys. Condens. Matter 1999, 11, A1
- [19] Sollich, P.; Lequeux, F.; Hbraud, P.; Cates, M. E. Phys. Rev. Lett. 1997 78 2020.

## Part II

# Thermo and pH responsive Microgel



## Chapter 7

# Temperature dependence of elasticity and dynamics of dense microgel suspensions

### 7.1 Introduction

Microgels are particles made by chemically cross-linking a polymer to form a gel with a colloidal size [1, 2]. Like for their macro-gel counterparts the particles can be swollen by a solvent, the degree of swelling depending on solvent quality [3]. Since the gel rigidity is usually determined by the cross-linking density, swelling leads to softness and deformability of the particle. In many cases the solvent quality may be controlled by external parameters making the microgels extremely versatile materials for applications like controlled drug delivery or to modify the rheological properties of pharmaceutical and industrial products [4, 5, 6]. In particular the size control of p-NIPA particles is very promising since p-NIPA has a low critical solution temperature (LCST) at about  $T \simeq 33^\circ\text{C}$ . So, by controlling the external parameters, it is possible to change the relative polymer-solvent and polymer-polymer interactions which in turn determine the swelling ratio. The internal structure and the swelling behavior of p-NIPA microgels have been extensively studied as function of temperature and cross-linking density [7, 8, 9, 10].

Unlike for their macro-gel counter parts, swollen microgel can be highly concentrated to form dense colloidal suspensions [11]. Experimentally, one finds that with colloidal suspensions made of rigid spherical particles, the volume fraction  $\phi$  for random close packing is  $\phi_{rcp} = 0.64$ . However, since microgels are swollen, one can continue packing well above  $\phi_{rcp}$  by compressing and deforming the particles. To describe the degree of packing and compression it is convenient to generalize the volume fraction  $\phi$  to  $\zeta = n \cdot v$ . Here,  $n$  is the particle number concentration and  $v$  the volume of the particle measured in dilute conditions ( $n \rightarrow 0$ ) with the same values

of the external parameters; with this definition  $\zeta = \phi$  when  $\zeta < 0.64$ . For  $\zeta$  close to, or above 1, a particle does not reach its swelling equilibrium because of the steric compression due to the other particles; in this case  $\zeta$  describes how much the particle is far from such equilibrium condition. At these high concentrations, the soft inter-particle repulsion leads to dynamics and viscoelastic properties that are reminiscent of those of pastes and colloidal glasses [12]. The key to the origin of elasticity in a dense repulsive microgel suspension is its dependence on  $\zeta$ . This intrinsic relationship and the microscopic mechanisms for elastic energy storage have only been suggested recently in analogy to emulsions [13]. For Pnipa microgel suspensions the viscosity and the linear viscoelastic moduli dependence on particle concentration and temperature have been studied below the LCST. In most cases the behavior of the zero-shear viscosity resembles that found for hard sphere suspensions once it is plotted against  $\zeta$  [7, 11, 14, 15]. For packed suspensions the elastic modulus  $G'$  shows a frequency independent plateau  $G'_p$ . It also seems that  $G'_p$  values measured at various temperature and weight concentrations, collapse on a single master-curve once plotted against  $\zeta$  [7, 11]. These re-scaling suggest that, at least below the LCST, temperature doesn't appreciably affect the inter-particle potential. In the case of Pnipa, however, the inter-particle interaction may be changed from repulsive to attractive by crossing the LCST. In fact it has been shown that above the LCST p-NIPA particles form aggregates [9]. However the effect of the attraction on the viscoelastic properties of concentrated suspensions is still unknown. In this work we show that the elasticity of p-NIPA dense suspensions exhibits critical-like behavior as function of temperature both above and below the LCST. Depending on temperature, the frequency dependence of the moduli reflects the behavior of a colloidal glass, a liquid and a colloidal gel. In the glassy state the moduli show qualitative analogies with hard sphere (HS) glasses and compressed emulsions [16, 17, 18]. In this region the elasticity scales with volume fraction as  $G' \sim (\zeta - \zeta_c)^\mu$ . The dynamic behavior of a liquid is un-expectedly reached at volume fractions above packing and for temperatures very close to the LCST, suggesting a change in the inter-particle interaction close to the transition temperature. Above the LCST particles become attractive and a whole space spanning network is formed, the elastic properties of this gel depending on temperature. Surprisingly, the elasticity in all the phases can be described by a common critical behavior with temperature, the critical temperature  $T_c$  being the LCST. Finally, this picture is somehow suggesting analogies between glass and gel phases.

## 7.2 Experimental

### 7.2.1 Particle synthesis and characterization methods

The microgel particles were synthesized with a standard precipitation polymerization method [2]. All reagents were purchased by Sigma Aldrich. A solution of 385 ml of water with 3.69 g N-isopropylacrylamide (NIPA), 0.029g N,N'-methylenebisacrylamide (BIS) and 0.29g Acrylic acid AAc was introduced in a 500 ml three necks flask equipped with a stirrer, nitrogen flow and water cooling. Under stirring the solution temperature was raised to 68 °C in a nitrogen saturated environment. When the solution reached the target temperature  $T \simeq 68^\circ\text{C}$  a solution of 10 ml water and 0.29g of initiator, potassium persulfate (KPS) was added. After about ten minutes from the introduction of the initiator, the solution became milky, indicating that colloidal nuclei were formed. The system was left reacting for five hours. At the end of the reaction the flask was removed from the oil bath and left cooling down to 25 °C. After extensive (about 15 days) dialysis against pure water, the microgel dispersion was freeze-dried. The resulting powder was then re-dispersed in water at 15% polymer weight fraction  $w_t\%$ . This solution was left in agitation at  $T \sim 27^\circ\text{C}$  for about 10 days to allow homogenization between the phases. Samples at different concentrations were then obtained by dilution from this batch.

The particle radius as function of temperature is determined in by Dynamic light scattering (DLS) using an ALV 5000 correlator and a laser of wavelength  $\lambda = 532\text{nm}$ . We use solutions at about 0.01% polymer mass which is dilute enough to avoid multiple scattering at all temperatures. At all temperatures we measure the intensity auto-correlation function  $f(q, t)$  at a wavevector  $q = 7.6\mu\text{m}^{-1}$ . At this small  $q$  the  $f(q, t)$  is well represented by a single exponential decay representing the Brownian motion of the spherical particle. For  $q \gtrsim 15$  this simple decay is lost and the  $f(q, t)$  becomes a more complex function suggesting that for these large values of  $q$  we are probing both the Brownian motion of the particle and its internal dynamics.

To measure the intrinsic viscosity of microgel solutions we use an Ubbelohde capillary immersed in a water bath. We can control the temperature of the bath with a precision of 0.01°C. The volume fraction at different temperatures is obtained by measuring the relative viscosity  $\eta/\eta_o$  of dilute suspensions at different polymer concentrations  $w_t$  as shown in figure 7.1. Using the Einstein-Batchelor relation  $\eta/\eta_o = 1 + 2.5(k \cdot w_t) + 6.2(k \cdot w_t)^2$  we fit the data at fixed temperature to obtain the intrinsic volume fraction  $k(T) = \phi/w_t$ .

The temperature dependences of both the particle volume  $V(T)$  and the intrinsic volume fraction  $k(T)$  are reported in figure 7.2. Let's observe that  $k = V/m_p$  where  $m_p$  is the average polymer mass per particle; for this reason  $k$  and  $V$  must have the same temperature dependence allowing for

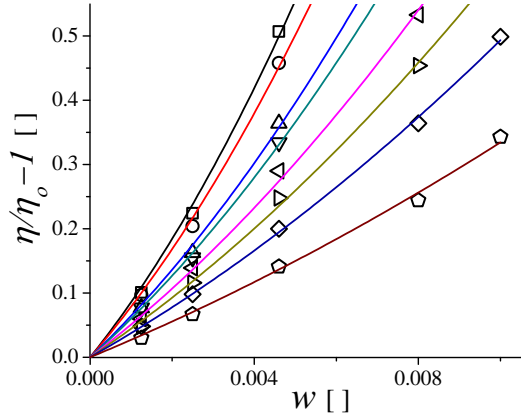


Figure 7.1: Dependence of the relative viscosity on polymer weight fraction  $w$  at different temperatures. The lines are fits to the data according to the Einstein-Batchelor model. From top to bottom the temperatures are 10,15, 20, 22, 24, 26, 28, 30  $^{\circ}C$

cross-checking the DLS and intrinsic viscosity measurements. In the inset of figure 7.2 we show that the linear relation between  $k$  and  $V$  is in fact respected and  $m_p$  can be extracted from the slope of this linear fitting.

Rheological measurements of concentrated dispersions are made with a Malvern Gemini HR nano rheometer using cone-plate geometry. We use a solvent trap that allows to obtain reproducible measurements over a couple of days. We have checked that our suspension is not affected by slip at the wall [19]. This is done by measuring flow curves for a fixed temperature and concentration with different surfaces. One roughened surface is obtained by sand blasting  $1\mu m$  PMMA particles on the cone and plates geometry. The other is a roughened aluminum parallel plate geometry. In any case we don't find any difference with the flat surface. The viscoelastic moduli  $G'$ ,  $G''$  are measured at a strain  $\gamma=0.01$  that is well inside the linear regime at all temperatures. Below the LCST, the linearity is lost for  $\gamma \gtrsim 0.03$  irrespective of temperature and polymer concentration. Above the LCST the linear viscoelastic range depends on concentration and temperature. We perform temperature scans of the samples fixing frequency  $\omega=1\text{rad/sec}$  and strain, and increasing temperature at  $0.2^{\circ}C/\text{min}$ . Once a given temperature is reached, samples may take a certain time to equilibrate or may even age [20], resulting in a time dependence of the viscoelastic properties. When performing frequency sweep tests we make sure that the measurement is reproducible when repeating it after 1 hour. Below the LCST, samples become stable after a few minutes that the target temperature is reached. Above

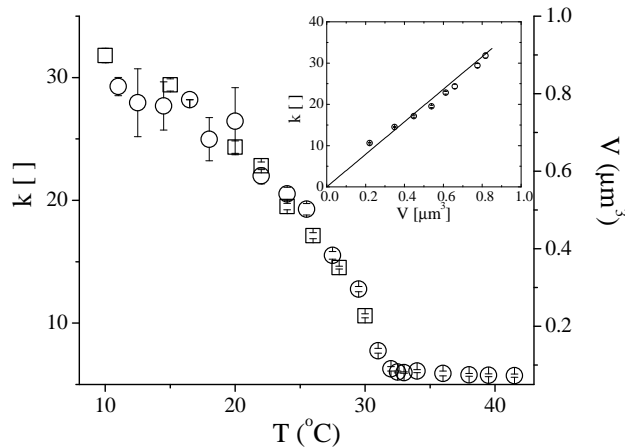


Figure 7.2: Temperature dependence of the intrinsic volume fraction  $k$  (squares) and particle volume (circles). The inset shows the linear relationship between the intrinsic volume fraction  $k$  and particle volume  $V$ . The slope of the linear fitting represents the inverse of the average mass of polymer per particle  $m_p$

the LCST instead, the viscoelastic moduli decrease in time over a period of about 1 hour. We show in the next section that at these temperatures the particles form a gel. Data are presented for samples left at constant temperature for more than 1 hour.

### 7.3 Results

To follow the temperature dependence of the linear viscoelastic moduli of a dense microgel suspension we fix the frequency and the strain applied to the sample and scan it by slowly varying temperature. A typical response is reported in figure 7.3 for a sample at a polymer weight fraction of  $0.062 \pm 0.005$  and a frequency  $\omega=1$  rad/sec.

The variation of volume fraction  $\zeta$  as measured both by DLS and viscosimetry is reported in the same figure. At low temperatures  $T \lesssim 26^\circ C$ , the elastic modulus dominates over the viscous one. As temperature increases in the range  $10 - 26^\circ C$  both moduli decrease and their difference gets smaller. Such a solid-like behavior and the absence of any visible Bragg-peak suggest that the suspension behaves like a glass. As temperature increases above  $26^\circ C$   $G'$  and  $G''$  become comparable.  $G''$  overcomes  $G'$  at  $T \sim 28^\circ C$  suggesting that the sample response is liquid-like. Interestingly  $\zeta$  is still above 0.64. Finally the moduli suddenly increase for temperatures higher than

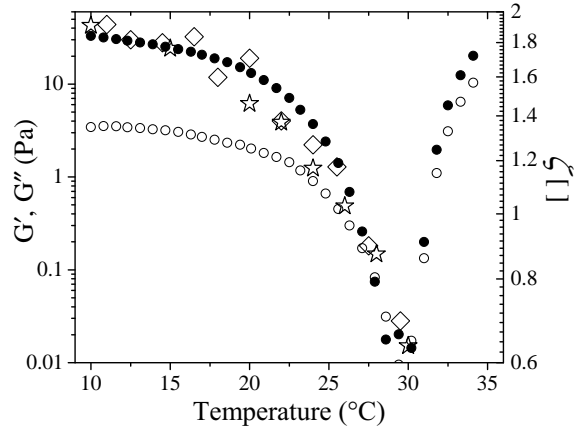


Figure 7.3: Temperature dependence of: linear viscoelastic moduli  $G'$  (solid circles) and  $G''$  (open circles); volume fraction  $\zeta$  as obtained by viscosity measurements (stars) and DLS (diamonds)

$30^{\circ}\text{C}$ . Around the LCST it's well known that the interaction changes from repulsive to attractive and cluster formation has been studied with p-NIPA microgels. We then expect a colloidal gelation induced by the attractive interaction between particles. As a consequence, the steep increase of the moduli reflects the increasing elasticity and dissipation of a particle network.

A better understanding of the dynamics in the different phases is obtained from the moduli frequency dependence. At low temperatures  $G'$  shows a frequency independent plateau and  $G''$  shows a marked minimum at a frequency  $\omega_m$ , as shown in figure 7.4 for three different temperatures. These features are characteristic of glassy dynamics of the suspension.

For  $\omega > \omega_m$   $G''(\omega)$  increases with frequency as  $G'' \propto \omega^{0.5}$ . Flow calculations predict this high frequency asymptotic dependence for concentrated suspensions of Brownian spheres interacting through a continuous repulsive potential [21]. Experiments with spherical particles stabilized by grafted polymer layers also suggest such a dependence [16, 22]. The increase of  $G''$  with decreasing  $\omega$  for  $\omega < \omega_m$  is reminiscent of HS glasses. Physically, this is due to the additional energy loss produced by a particle when escaping from the cage induced by the surrounding neighborhoods. It reflects the increasing dissipation that generates approaching the structural relaxation. At the glass-transition volume fraction  $\zeta_g \approx 0.58$  an HS suspension loses its low frequency relaxation and becomes non-ergodic. This implies a finite, ideal zero-frequency elastic modulus and no rise in  $G''(\omega)$  toward low  $\omega$ . Instead our microgel suspension shows evidence of a low-frequency relaxation even for volume fractions  $\zeta \gg \zeta_g$  where the particles are highly compressed. This

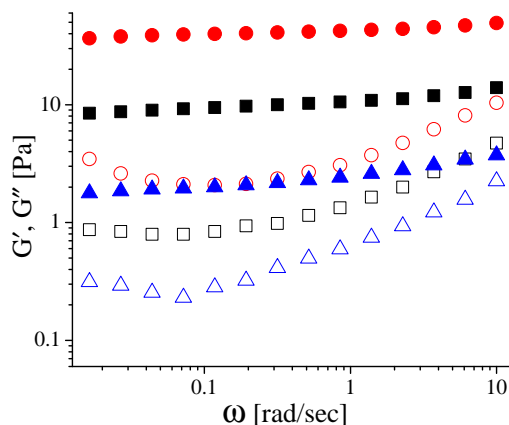


Figure 7.4: Frequency dependence of the elastic  $G'$  (solid symbols) and viscous  $G''$  (open symbols) moduli in the glassy region. Circles, squares and triangles indicate temperatures of 10, 20 and 24 °C respectively

difference suggests that the non-zero compressibility and deformability of the particles allow for persistent relaxation through rearrangements. Qualitatively, the measured frequency dependencies of  $G'(T, \omega)$  and  $G''(T, \omega)$  for concentrated, swollen microgels, resemble those of glassy hard spheres and concentrated emulsions suspensions [16, 17]. However the origin of the elastic response is different. In HS the elasticity is entropic, stemming from the different relative particle configurations at and out of equilibrium. In emulsions such an entropic contribution is expected up to  $\zeta_g$ . From this point the droplets start deforming and the elasticity linearly increases with volume fraction as  $G' \sim \zeta - \zeta_c$ ; this is due to the energy associated to the additional surface area created by deformation, which opposes to Laplace pressure and to the random microstructure of the system [17, 23]. Surprisingly, in this region the shear modulus is nearly the same as the osmotic pressure  $\Pi$ ,  $G' \cong \Pi$ , whereas the bulk modulus shows a discontinuity at  $\zeta_g$ . This behavior persists up to  $\zeta \lesssim 1$  that is the dry foam limit.

On the other hand, swollen microgels may deform and compress and, as a consequence, they can be packed at generalized volume fractions well above 1 as shown in figure 7.3.

For  $0.64 \lesssim \zeta \lesssim 1$  we expect the particles to deform without changing their volume. In fact far from the transition point of the gel, the bulk modulus  $B$  of a particle is higher than the particle shear modulus [24]. As a consequence particles will form facets at contact. This microscopic picture is analogous to that for emulsions suggesting that in this region  $G' \sim (\zeta - \zeta_c)$  [13]. At  $\zeta \approx 1$  however, the particles start deswelling. It has been suggested

that in this region, the suspension elasticity increases as a consequence of the increasing bulk modulus of the single particle as it de-swells with increasing concentration [13].

At temperatures above 25 °C the suspension dynamics changes. Both  $G'$  and  $G''$  show a frequency dependence that becomes more marked as temperature increases. This is plotted in figure 7.5 for three different temperatures.

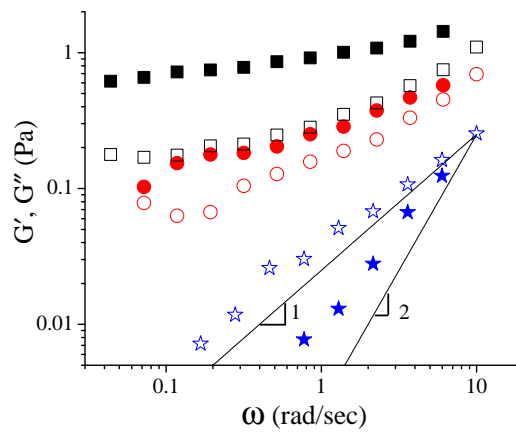


Figure 7.5: Frequency dependence of the linear viscoelastic moduli  $G'$ (solid) and  $G''$ (open) as function temperature: 26 °C (squares), 27 °C (circles), 28°C (stars). The solid lines show the terminal behavior of a viscoelastic liquid

Although at 26°C the  $G'$  frequency dependence is weak, it becomes marked at 27°C where a structural relaxation is evident for  $\omega \sim 0.1$  rad/sec. Finally at 28°C the frequency dependences of both moduli, approach the terminal behavior of a viscoelastic liquid,  $G' \sim \omega^2$  and  $G'' \sim \omega^1$  reflecting the liquid-like nature of the sample.

Above the LCST, the moduli frequency dependence changes. We find that both  $G'$  and  $G''$  are characterized by a power law of the type  $G \sim \omega^{0.3}$  in the whole frequency range investigated. Such a dependence is reported in figure 7.6 for three different temperatures. A power law relaxation spectrum characterizes transient particle networks [30] and in particular gel characterized by a long range attractive potential [27].

At these high temperatures, the inter-particle attraction is related to the Flory parameter  $\chi$  which increases with temperature. The observed increment of the moduli is a direct consequence of the increasing attraction [25] with temperature. Unexpectedly the ratio between the moduli  $G''/G' = \tan \delta \approx 0.6$  remains almost constant with attraction and frequency. This is quite different from classical colloidal gels of rigid particles where,

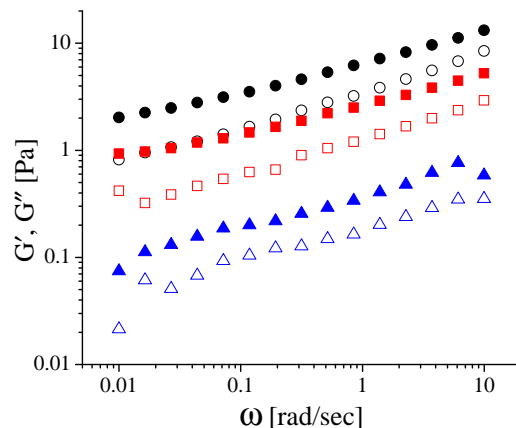


Figure 7.6: Frequency dependence of  $G'$  (solid) and  $G''$  (open) as function of temperature, after an aging time of 150 minutes.  $T= 35$  °C (circles),  $T= 33$  °C (squares),  $T= 31$  °C (triangles)

increasing attraction, increases the elasticity of the network interdispersed within the liquid, while keeping dissipation almost constant [26, 27]. There are two main differences in the structural properties of gels of microgels and classical colloidal gels of solid particles. One, is that even at high temperatures a microgel particle contains a high amount of water so that the total friction between gel and water is higher than expected for impermeable particles. Second, P-Nipa particles form stable aggregates which size depends on temperature. As a consequence, we expect the elasticity to arise as the result of crowding of stable clusters rather than from an incipient cluster that spans the whole volume [28]. Within this picture, for these peculiar particles gelation would be more likely interpreted as a glass of clusters rather than an arrested state produced during spinodal decomposition [29].

## 7.4 Critical behavior at the LCST

The previous analysis highlights an unexpected behavior around the LCST. In fact we have shown that the liquid phase can be reached with  $\zeta$  still being above packing. This suggests that, in contrast to hard spheres,  $\zeta$  is not the only variable depending on temperature and determining the mechanical response. To better focus on this phenomenon, we analyze the variation of the elastic modulus plateau  $G'_p$  as function of temperature. This is plotted in figure 7.7 for two different polymer concentrations, 0.062 and 0.112. Close to the liquid state, where  $G'$  does not show a plateau,  $G'_p$  is taken as the

inflection point of the elastic modulus. In the gel state we choose to take  $G'_p$  as the value of  $G'$  at 0.1 rad/sec. Not too far from the LCST the data are well fitted to the equation  $G'_p \sim (T - T_c)^\gamma$  describing critical behavior. While  $\gamma$  increases with polymer content, we find that the critical temperature  $T_c$  remains almost constant:  $T_c \simeq 29^\circ\text{C} \simeq \text{LCST}$ .

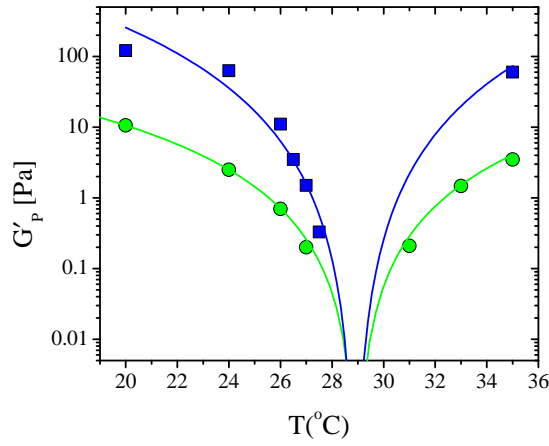


Figure 7.7: Temperature dependence of  $G'_p$  at two different polymer concentrations: 0.062 (circles) and 0.112 (squares). The lines are fitting to the equation  $G'_p = A(T - T_c)^\gamma$

The independence of  $T_c$  on  $\zeta$  supports our idea that approaching the LCST the rheological response is controlled by a decreasing repulsive potential. However, we recognize that here the rheological moduli are subject to the effect of decreasing both the inter-particle repulsion and  $\zeta$ . In a quantitative analysis, aiming to extrapolate the temperature dependence of the repulsive potential,  $\zeta$  should be fixed. This can be done, for example, by measuring  $G'_p$  for different temperatures and polymer concentrations. As consequence of a varying potential, the  $G'_p$  should not scale on a single curve when plotted as function of  $\zeta$ . In figure 7.8, in fact, we observe that not all the values of  $G'_p$  scale on a single curve, the deviations appearing for the sample at the highest polymer concentration and for temperatures close to  $T_c$ . Finally, a surprising frequency response is found for dense samples at  $28^\circ\text{C}$ . At this temperature it is not possible to determine a value for  $G'_p$  since the samples display a liquid-like rheological response which is independent on  $\zeta$ . This remarkable behavior is shown in the inset of figure 7.8 for two concentrations above packing.

Although we have extensively shown that the inter-particle repulsion depends on temperature and decreases close to the LCST, the reason deter-

mining this unexpected response is still unknown. One possibility is related to the softening of a single particle bulk modulus at the LCST. Hirotsu [24] has measured the bulk and shear moduli on p-Nipa hydrogels. He found that at the LCST the shear modulus increases while the bulk modulus drops down to zero as predicted by the theory of Flory. In a concentrated, disordered suspension of repulsive particles, the link between the elastic properties of the single particle and the longitudinal and transverse components of the stress of the suspension as a whole are, however, still controversial [13, 23]. As a consequence our hypothesis, remains a conjecture. However we hope that our findings will promote more experimental and theoretical works aiming to elucidate the peculiar elastic behavior at the transition and the microscopic origins of the fascinating elastic properties of these materials.

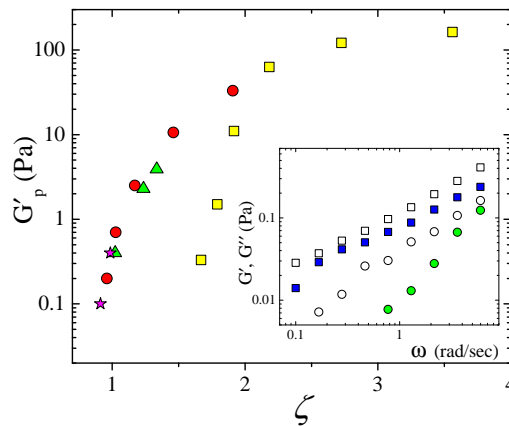


Figure 7.8: Dependence of  $G'_p$  on  $\zeta$  for different polymer concentrations and temperatures. For each polymer concentration the temperatures are reported from top to bottom: 0.112 (squares: 10, 20, 24, 26, 27, 27,5 °C); 0.062 (circles: 10, 20, 24, 26, 27 °C); 0.042 (triangles: 10, 15, 20 °C); 0.031 (stars: 15, 20°C). The inset shows the frequency dependence of the linear viscoelastic moduli for two samples at polymer concentrations of 0.112 ( $\zeta=1.62$ ) (squares) and 0.062 ( $\zeta=0.87$ ) (circles) at  $T=28$  °C.

## 7.5 Conclusions

The viscoelastic properties of a concentrated suspension of temperature-sensitive microgel particles have been analyzed. The system experiences rheological transitions, showing glass, liquid and gel like dynamics as temperature is increased. Although volume fraction plays an important rule, it

does not seem to be the only parameter determining the macroscopic mechanical response of the system. As expected, in the gel state the effective inter-particle potential is the key-parameter determining the viscoelastic response. This phase, may only partially be described within the general framework of attractive colloids. Surprisingly, we have found that also in the transition between glassy and liquid states, the elasticity may not be described within the framework of hard spheres. Even by adjusting for effective volume fraction, we found the elastic modulus to be orders of magnitude smaller than expected for hard spheres. We pointed out that temperature might not just be playing a mere volume fraction effect, but effectively changing the inter-particle potential, for example by changing the bulk modulus of the particles.

# Bibliography

- [1] G. Chen and A. S. Hoffman, *Nature (London)*, 373, 49 (1995)
- [2] M. J. Snowden, B. Z. Chowdhry, B. Vincent, and G. E. Morris *J. Chem. Soc. Faraday Trans. 92*, 5013 (1996)
- [3] Y. Hirose, T. Amiya, Y. Hirokawa, and T. Tanaka *Macromolecules* 20, 1342 (1987)
- [4] N. A. Peppas, *R. Langer Science* 263, 1994, 1715
- [5] Brannon-Peppas L. *Absorbent polymer technology* Elsevier: Amsterdam 1990; pp45
- [6] C. M. Nolan, C. D. Reyes, J. D. Debord, A. J. Garcia, and L. A. Lyon *Biomacromolecules* 6, 2032 (2005)
- [7] H. Senff, W. Richtering *Colloid Polym Sci* 278, 830 (2000)
- [8] M. Stieger, W. Richtering, J. S. Pedersen, P. Lindner, *J Chem Phys* 120, 6197 (2004)
- [9] K. Kratz, T. Hellweg, W. Eimer *Colloids and surfaces A* 170, 137 (2000)
- [10] A. Fernandez-Barbero, A. Fernandez-Nieves, I. Grillo, and E. Lopez Cabarcos *Phys. Rev. E* 66, 051803 (2002)
- [11] H. Senff, W. Richtering *J Chem Phys* 111-1705 (1999)
- [12] M. Cloitre, R. Borrega, F. Monti, and L. Leibler *Phys. Rev. Lett.* 90, 068303 (2003)
- [13] J. R. Seth, M. Cloitre, R. T. Bonnecaze *J. Rheol.* 50, 353 (2006)
- [14] M. Stieger, J. S. Pedersen, P. Lindner, W. Richtering *Langmuir* 20-7283 (2004)
- [15] B. H. Tan, K. C. Tam, Y. C. Lam, C. B. Tan *J. Rheol* 48, 915 (2004)
- [16] T. G. Mason and D. A. Weitz, *Phys. Rev. Lett.* 75, 2770 (1995)

*Chapter 7*

---

- [17] T. G. Mason and D. A. Weitz, Phys. Rev. Lett. 75, 2051 (1995)
- [18] T. G. Mason, Martin-D. Lacasse, Gary S. Grest, Dov Levine, J. Bibette, and D.A. Weitz, Phys. Rev. E 56, 3150 (1997)
- [19] S. P. Meeker, R. T. Bonnecaze, and M. Cloitre Phys. Rev. Lett. 92, 198302 (2004)
- [20] M. Cloitre, R. Borrega, and L. Leibler Phys. Rev. Lett. 85, 4819 (2000)
- [21] R. A. Lionberger and W. B. Russel J. Rheol. 38, 1885 (1994)
- [22] J. van der Werff, C. de Kruif, C. Blom, and J. Mellema Phys. Rev. A 39, 795 (1989)
- [23] Martin-D. Lacasse, Gary S. Grest, Dov Levine, T. G. Mason, and D.A. Weitz, Phys. Rev. Lett. 76, 3448 (1996)
- [24] S. Hirotsu Phase Transitions 47, 183-200 (1994)
- [25] V. Trappe, V. Prasad, Luca Cipelletti, P.N. Segre, and D. A. Weitz Nature 411, 772 (2001)
- [26] V. Trappe, and D. A. Weitz 85, 449 (2000)
- [27] V. Prasad, V. Trappe, A. D. Dinsmore, P. N. Segre, L. Cipelletti, and D. A. Weitz faraday Discussions 123, 1 (2003)
- [28] G. Romeo, G.Filippone, A. Fernndez-Nieves, P. Russo, and D. Acierno Rheol. Acta
- [29] P. J. Lu, E. Zaccarelli, F. Ciulla, A. B. Schofield, F. Sciortino, and D. A. Weitz Nature Letters 453, 499 (2008)
- [30] W. Walters, D. van den Ende, V. Breedveld, M. H. G. Duits, A. Potanin, R. H. H. Wientjes, and J. Mellema Phys. Rev. E 56, 5726 (1997)

# Chapter 8

## Microscopic dynamics

### 8.1 Introduction

Colloidal dispersions display transitions similar to those observed in atomic or molecular systems [1]. Although such phase transitions have been studied for decades, predictions of phase diagrams are not always realized because the systems remain kinetically trapped in out of equilibrium states. Discrepancies between predictions and actual observations rely on the intricacies of the dynamics of phase transitions. Recent advances in optical and imaging techniques have allowed at looking directly at particle movement in colloidal samples; fundamental insights into the structure of the metastable states and the underlying mechanisms of their local dynamics have been obtained [2, 3]. One of the most intriguing out of equilibrium states which is common to a variety of systems is the glass. Understanding the microscopic dynamics underlying the kinetic arrest during the approach to the glassy state is an important scientific goal. If the colloidal particles interact with a simple Hard Sphere (HS) potential, the only thermodynamic variable is the particle volume fraction  $\phi$ ; even in this simple case the system experiences phase transitions and may remain trapped in a glassy state as shown in figure 8.1.

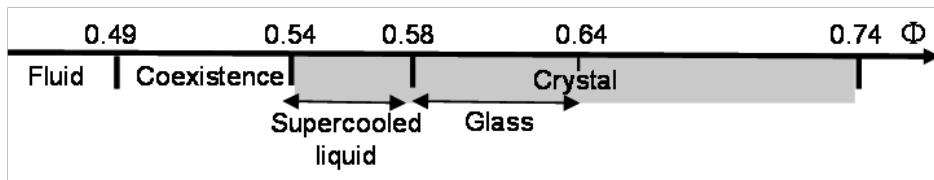


Figure 8.1: Phase diagram of a dispersion of hard spheres. Both equilibrium and out of equilibrium phases are reported together with phase boundaries.

Studies of optical microscopy on colloidal supercooled liquids HS have

shown the presence of domains of particles which, through cooperative motion, bring to local rearrangements. The resulting dynamic heterogeneities among particles are maximum at the relaxation time, proving the importance of local dynamics on structural relaxation of super-cooled liquids.

A soft repulsive potential may be introduced by using compressible colloidal particles; micro-particles made of a polymer gel suspended in a good solvent combine the nanoscopic characteristics of a gel with a microscopic colloidal behavior. The microgel compressibility introduces an intrinsic energetic scale which is absent in HS systems. Boundaries between phases and transport properties are greatly affected by the introduction of a finite bulk modulus if compared to hard spheres [4]. The use of microgel colloidal particles has many advantages: because the particles exist in the swollen state, both density and index of refraction are homogeneous throughout the system. Those are ideal conditions to avoid buoyancy and reduce inter-particle attraction [5]. The latter is also the optimal condition to work with microscopy techniques.

The high degree of swelling allows concentrating microgel suspensions at volume fractions  $\zeta > 1$ ; this is reflected in a compression of each particle. Highly concentrated suspensions have been used as model systems to study glassy dynamics and ageing phenomena common to many different materials [6] and to find correlations between microscopic dynamics and bulk rheology in the glassy state. However the most complex and intriguing dynamics in the approach to the glass are observed in the supercooled liquid state.

In this contribution we study the dynamics of soft repulsive particles at different volume fractions focusing on the behavior of the supercooled liquid. Local dynamics, on the single particle scale, are obtained through dynamic light scattering (DLS) and confocal microscopy (CM) studies. By increasing  $\zeta$ , we increase the degree of compression and observe complex particle dynamics. From confocal data we may extract the particles displacement distribution, from which we observe non-Gaussian statistics for the dynamics in the deeply quenched supercooled liquid.

## 8.2 Experimental

The particles' synthesis was described in the previous chapter. Rhodamine monomer was added during the polymerization to obtain fluorescent particles. At  $pH > 6$  and low salt concentrations ( $[NaCl] \simeq 10^{-4}$  M) the charged groups of the acrylic acid are almost all dissociated and the particles remain fully swollen at all temperatures because of the osmotic pressure induced by the counter-ions in the gel network. All the experiments were conducted at temperature  $T \simeq 20^\circ C$  on samples at  $8 < pH < 9$ , so that temperature fluctuations and small pH differences between samples at different concentrations do not affect particle dimensions [7].

An ALV CGS-3000 light scattering apparatus was used to measure the time averaged intensity correlation function  $\langle g^2(k, \tau) \rangle_t$  of the light scattered by the particles in homodyne experiments. Here  $k$  is the wavevector and  $\tau$  the lag-time. The incident beam is a laser with wavelength  $\lambda = 633 \text{ nm}$ .

From  $\langle g^2(k, \tau) \rangle_t$ , the ensemble averaged electric field correlation function  $\langle g^1(k, \tau) \rangle_E$  can be extracted. Assuming the range of correlation between particle positions much smaller than  $V^{1/3}$ , with  $V$  the scattering volume, the instantaneous electric field of the scattered light is a zero mean Gaussian variable [8]. This measures the intermediate scattering function or dynamic structure factor  $F(\mathbf{k}, \tau)$  which is the quantity of interest. For ergodic systems time and ensemble averages are the same and from the Siegert relation [8] the ensemble averaged field correlation function is obtained by the time average of the intensity correlation function:  $F(\mathbf{k}, \tau) = \langle g^2(k, \tau) \rangle = 1 + [\langle g^1(k, \tau) \rangle]^2$ . For non-ergodic samples the ensemble averages may be obtained by measuring the intensity of the light scattered by different sub-ensembles of the sample (for example by changing the position of the vial with respect to the incident beam) and then averaging. However, a much simpler and less tedious procedure was suggested by Pusey and van Meegen [9] and is used here.

To analyse a light scattering experiment it is necessary to construct a particular model for the dynamic structure factor. In many cases this is a formidable task that is generally resolved by making a number of assumptions which can be more or less justified. In the present case we are mainly interested to extract the self dynamic structure factor from which the particle mean square displacement can be easily obtained. Here we use a very simple model: non-interacting scatterers restricted by the neighborhoods of random fixed positions by weak harmonic forces.

For identical scatterers,  $F(\mathbf{k}, \tau)$  reduces to

$$F(\mathbf{k}, \tau) = \sum_{j=1}^N \sum_{k=1}^N \langle \exp\{i\mathbf{k} \cdot [\mathbf{r}_j(0) - \mathbf{r}_k(\tau)]\} \rangle_E \quad (8.1)$$

where  $N$  is the number of scatterers in the volume and  $\mathbf{r}_j, \mathbf{r}_k$  the particle positions. It's useful to define a normalised dynamic structure factor by:

$$f(\mathbf{k}, \tau) = F(\mathbf{k}, \tau) / F(\mathbf{k}, 0) \quad (8.2)$$

Let's observe that for  $k \cdot R > 1$ ,  $F(\mathbf{k}, 0) = 1$ , where  $R$  is the particle radius. For non-interacting scatterers,  $\langle g^1(k, \tau) \rangle_E$  expresses the self dynamic structure factor [8]

$$f(\mathbf{k}, \tau) = \frac{1}{N} \sum_{j=1}^N \langle \exp\{i\mathbf{k} \cdot [\mathbf{r}_j(0) - \mathbf{r}_j(\tau)]\} \rangle_E \quad (8.3)$$

If the particle displacements  $r$  are Gaussian variables (which is actually the case for weak harmonic forces), the particle MSD  $\Delta r^2(\tau)$  can be extracted from [9]

$$f(\mathbf{k}, \tau) = \exp\{-(k^2/6) \cdot \langle \Delta r^2(\tau) \rangle\} \quad (8.4)$$

We have verified that this relation holds in concentrated samples. This is shown in figure 8.2 where the mean square displacements for a sample at polymer concentration of 0.56%, which is in the concentrated regime, are plotted as function of lag-time  $\tau$  for different wavevectors. The relative electric field correlation functions  $\langle g^1(k, \tau) \rangle_E$  from which the MSD are extracted are reported in the inset of figure 8.2.

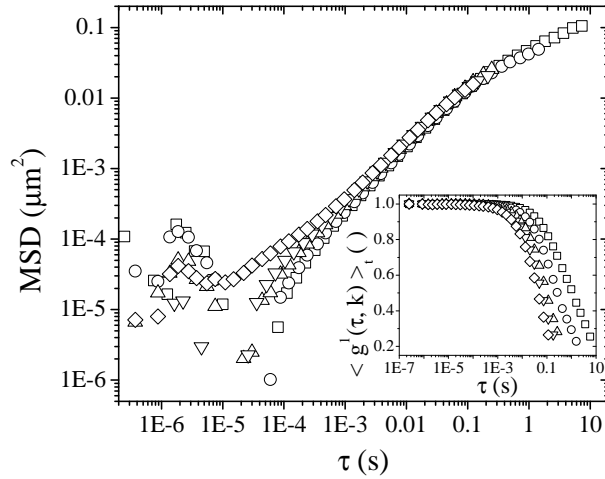


Figure 8.2: MSD curves for different wavevectors  $k(1/\mu m)$ .  $k=9$  (squares), 13.2 (circles), 17 (triangles), 20.2 (reverse triangles), 22.9 (diamonds) as a function of lag-time  $\tau$ . In the inset the time average correlation function of the electric field is reported as function of lag-time. Symbols are the same of the main plot.

Although the  $k^2$  scaling is respected, the assumption of non-interacting scatterers, leading to equation 8.3 remains quite unjustified.

A confocal microscope (Zeiss) was used to capture sequences of images in time at a fixed focal plane which was always at least  $15 \mu m$  far from the glass. The particle tracking software written by Crocker [10] was used to determine the locations of the center of mass of the fluorescent particles in each frame and then to construct the particle trajectories.

Particle volume fractions are calculated as  $\zeta = Aw$  where  $w$  is the polymer weight fraction and  $A$  a proportionality constant.  $A = 218$  is obtained

from a fit to the suspension relative viscosity  $\eta_{rel}$  at low volume fractions, with the Batchelor equation

$$\eta_{rel} = 1 + 2.5\zeta + 6.2\zeta^2 \quad (8.5)$$

### 8.3 Results

Different mechanisms for particle dynamics are observed as  $\zeta$  changes. In figure 8.3 the mean square displacement is reported as function of lag-time in a double logarithmic plot. At  $\zeta=0.02$ , a slope of the MSD curve equal to 1 expresses a purely diffusive particle dynamic at all time intervals in dilute regime. An example of particle trajectory shows that the motion is in fact a random walk. At  $\zeta=0.5$  the dynamic is still diffusive at all times. In HS systems at this volume fraction, hydrodynamic and direct interactions between particles reduce the diffusion coefficient of a factor 50 with respect to the dilute case [11]. We find that the reduction is just a factor of 3 in our case, reflecting the extreme softness of the particles [12].

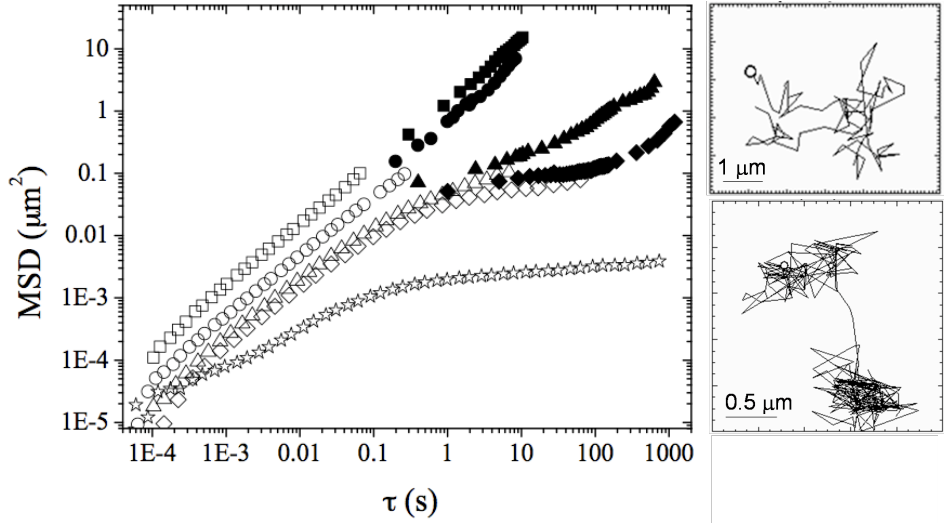


Figure 8.3: Left: Dependence of the MSD on lag-delay time  $\tau$  for particle volume fractions  $\zeta = 0.02$  (squares);  $0.5$  (circles);  $1.22$  (triangles);  $1.96$  (diamonds);  $2.77$  (stars). Empty symbols are from DLS and solid symbols from CM. The images on the right represent particle trajectories at  $\zeta = 0.02$  (top) and  $\zeta = 1.96$  (bottom) of duration 26 and 500 seconds respectively.

At  $1 < \zeta < 2$  we observe dynamics typical of supercooled liquids. At short time scales particle motion is diffusive but, as displacement becomes large enough, the presence of a cage formed by the neighboring particles determines a constraint to the motion. This is manifested by an inflection

in the MSD at  $\zeta=1.22$  but becomes a plateau that extends over two decades in time as  $\zeta$  increases to 1.96. Cage rearrangement leads to an upturn in MSD at the end of the plateau and at even longer lag-times, the motion again becomes diffusive: this behavior is known as cage-effect. This picture is confirmed by inspection of a particle trajectory, as reported in figure 8.3, showing both motion in the cage and cage rearrangement. For higher volume fractions the behavior is sub-diffusive even at the shortest time-scales and cage rearrangement is not observed; the system is trapped in a glassy state. In HS systems it has been shown that the presence of cage effect is manifested through a heterogeneity among particles' dynamics: at a fixed lag-time, particles involved in cage rearrangements are allowed to move over longer distances than trapped particles. Since particles behavior is inhomogeneous, displacements at fixed lag-times have a non-Gaussian distribution. Deviations from gaussianity can be used to quantify cage effect through the non-Gaussian parameter

$$\alpha_2(\tau) = \frac{\langle \Delta x^4 \rangle}{3 \langle \Delta x^2 \rangle^2} - 1 \quad (8.6)$$

with  $\Delta x$  the one-dimensional displacement.  $\alpha_2$  is zero for a perfectly gaussian distribution, while it increases as the distribution deviates from gaussianity. As shown in figure 8.4  $\alpha_2$  remains close to zero at all  $\zeta$  except for the deeply quenched supercooled liquid.

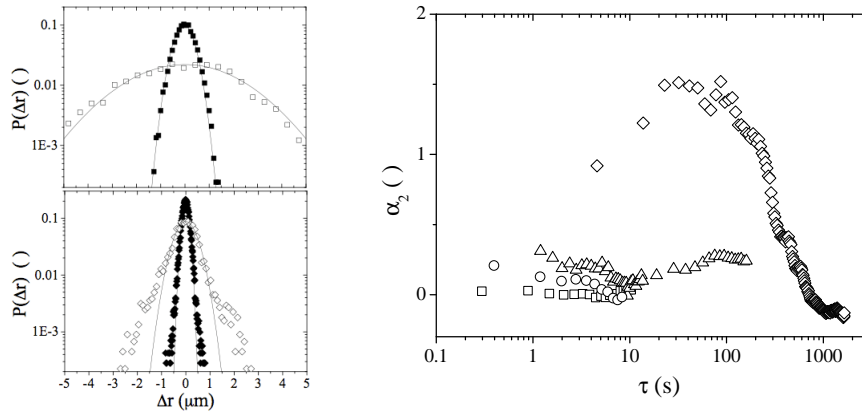


Figure 8.4: Left: displacement distributions for samples at  $\zeta=0.02$  (top) and  $\zeta=1.96$  (bottom). Lines are Gaussian fits to the data. For each sample, solid and empty symbols are for shorter and longer  $\tau$  values respectively. Right: Non Gaussian parameter  $\alpha_2$  for samples at different  $\zeta$  as function of lag-time. Symbols are the same as in figure 8.3

At  $\zeta=1.96$ ,  $\alpha_2$  strongly depends on lag-time; it shows a maximum for

$\zeta \simeq 100$  seconds, comparable to the relaxation time scale. This behavior suggests that dynamic heterogeneities, and hence cage rearrangement, are greatest at the relaxation time, emphasizing the fundamental rule played by local rearrangements in the structural relaxation.

Chapter 8

# Bibliography

- [1] V. J. Anderson, H. N. W. Lekkerkerker Nature, 416, 811 (2002).
- [2] Weeks E. R., Crocker J. R., Levitt A. C., Schofield A. and Weitz D. A. Science 287, 627 (2000)
- [3] P.J. Lu, E. Zaccarelli, F. Ciulla, A.B. Schofield, F. Sciortino, D.A. Weitz, Nature, 453, 499 (2008)
- [4] H. Senff, W. Richtering Colloid Polym Sci 278, 830 (2000)
- [5] Israelachvili, J. *Intermolecular and surface forces* Second edition, Elsevier (1992)
- [6] M. Cloitre, R. Borrega, F. Monti, and L. Leibler Phys. Rev. Lett. 90, 068303 (2003)
- [7] A. Fernandez-Nieves, A. Fernandez-Barbero, B. Vincent, and F. J. de las Nieves Macromolecules 33, 2114 (2000)
- [8] Dhont J. K. G. *An introduction to dynamics of colloids*, Elsevier (1996)
- [9] Pusey P.N., van Megen W. Physica A 157, 705 (1989)
- [10] J.C. Crocker and D. G. Grier, J Colloid Interface Sci, 179, 298 (1996)
- [11] P.N. Segrè, S.P. Meeker, P.N. Pusey and W. C. K. Poon, Phys Rev Lett 75, 958 (1995)
- [12] S. Pyett, W. Richtering, J Chem Phys 122, 34709 (2005)